T.C.

ABANT IZZET BAYSAL UNIVERSITY

THE GRADUATE SCHOOL OF NATURAL AND APPLIED SCIENCES

DESIGN AND BEAM DYNAMICS STUDIES FOR 5 GEV ELECTRON LINAC IN CLIC POSITRON SOURCE

MASTER OF SCIENCE

UMUT KESKİN

BOLU, MAY 2018

T.C.
ABANT IZZET BAYSAL UNIVERSITY
THE GRADUATE SCHOOL OF NATURAL AND APPLIED SCIENCES
THE DEPARTMENT OF PHYSICS

DESIGN AND BEAM DYNAMICS STUDIES FOR 5 GEV ELECTRON LINAC IN CLIC POSITRON SOURCE

MASTER OF SCIENCE

UMUT KESKİN

BOLU, MAY 2018

APPROVAL OF THE THESIS

DESIGN AND BEAM DYNAMICS STUDIES FOR 5 GEV ELECTRON LINAC IN CLIC POSITRON SOURCE submitted by **UMUT KESKİN** in partial fulfillment of the requirements for the degree of Master of Science in Department of Physics, **The Graduate School of Natural and Applied Sciences of ABANT IZZET BAYSAL UNIVERSITY in** 21/05/2018 by

Examining Committee Members	**Signature**
Supervisor Prof. Dr. Haluk DENİZLİ Abant İzzet Baysal University	....
Member Assoc. Prof. Dr. Abdulkadir ŞENOL Abant İzzet Baysal University	....
Member Assist. Prof. Dr. Ali YILMAZ Giresun University	....

Graduation Date :

Assoc. Prof. Dr. Ömer ÖZYURT ....

Director of Graduate School of Natural and Applied Sciences

To My Family

DECLARATION

I hereby declare that all information in this document has been obtained and presented in accordance with academic rules and ethical conduct. I also declare that, as required by these rules and conduct, I have fully cited and referenced all material and results that are not original to this work.

Umut KESKİN

ABSTRACT

DESIGN AND BEAM DYNAMICS STUDIES FOR 5 GEV ELECTRON LINAC IN CLIC POSITRON SOURCE
MSC THESIS
UMUT KESKİN
ABANT IZZET BAYSAL UNIVERSITY GRADUATE SCHOOL OF NATURAL AND APPLIED SCIENCES
DEPARTMENT OF PHYSICS
(SUPERVISOR: PROF. DR. HALUK DENİZLİ)
BOLU, MAY 2018

CLIC (Compact Linear Collider) and ILC (International Linear Collider) are the two future linear collider projects after LHC (Large Hadron Collider) era. Both are planning to accelerate electrons and positrons to collide at a centre-of-mass energy greater than 250 GeV. CLIC is foreseen to be constructed in several stages corresponding to different centre-of-mass energies. The first at 380 GeV would be followed by stages at 1.5 and 3 TeV. What makes CLIC unique is the two-beam acceleration scheme. Drive beam reaching a current of about 100 A at a beam energy of about 2.4 GeV is transported through the main linac tunnel and power both main electron and positron beams. One of the most important part is injection of main beams to the main linac tunnel. Electrons are produced by an electron gun and transport through different energy linacs to the main linac. For the positron production, 5 GeV electron beam is planned to be used by impinging to amorphous tungsten target. This thesis is based on the design and optimization of parameters as well as effect of instabilities on designed beamline for this 5 GeV electron linac for positron production chain.

Keywords: Accelerator, Collider, Linac, Compact Linear Collider, Positron Beam, Electron Beam, Beam Injector

ÖZET

CLIC POZİTRON KAYNAĞINDAKİ 5 GEV ELEKTRON DOĞRUSAL HIZLANDIRICISI İÇİN TASARIM VE DEMET DİNAMİĞİ ÇALIŞMALARI
YÜKSEK LİSANS TEZİ
UMUT KESKİN
ABANT İZZET BAYSAL ÜNİVERSİTESİ FEN BİLİMLERİ ENSTİTÜSÜ
FİZİK ANABİLİM DALI
(TEZ DANIŞMANI: PROF. DR. HALUK DENİZLİ)
BOLU, MAYIS 2018

CLIC (Kompakt Doğrusal Hızlandırıcı) ve ILC (Uluslararası Doğrusal Hızlandırıcı), LHC (Büyük Hadron Çarpıştırıcısı) döneminden sonra gelecekte yapılması planlanan iki doğrusal çarpıştırıcı projesidir. Her iki projede, 250 GeV'den daha büyük bir kütle merkezi enerjisinde çarpışacak olan elektron ve pozitronların hızlandırılması planlanmaktadır. CLIC'in farklı kütle merkezi enerjili birkaç aşamadan oluşturulması öngörülmektedir. İlk olarak 380 GeV, daha sonra bunu 1.5 ve 3 TeV aşamaları takip edecektir. CLIC'i benzersiz yapan şey iki demetli hızlanma şemasıdır. Sürücü demeti yaklaşık olarak 100 A'lik bir akımda 2.4 GeV ışın enerjisine ulaşır ve ana doğrusal hızlandırıcıya taşınarak elektron ve pozitron demetlerine güç sağlar. Burada en önemli parçalardan biri ise ana ışınların ana doğrusal hızlandırıcı tünellerine aktarılmasıdır. Elektronlar bir elektron tabancasıyla üretilir ve ana doğrusal hızlandırıcıya farklı ışın enerjisindeki doğrusal hızlandırıcılar vasıtasıyla taşınır. Pozitron üretimi için ise 5 GeV ışın enerjili bir elektron demetinin tungsten hedefe çarptırılarak kullanılması planlanmaktadır. Bu tez çalışması, pozitron üretim zinciri için tasarlanan 5 GeV demet enerjili elektron doğrusal hızlandırıcısının tasarımı, parametrelerinin optimizasyonu ve demet hattındaki bozuklukların, tasarlanan yapıyı nasıl etkilediğinin incelenmesine dayanmaktadır.

Anahtar Kelimeler: Hızlandırıcı, Çapıştırıcı, Doğrusal Hızlandırıcı, Kompakt Doğrusal Hızlandırıcı, Pozitron Işını, Elektron Işını, Işın Enjektörü

TABLE OF CONTENTS

Page

LIST OF FIGURES

Page

LIST OF TABLES

Page

LIST OF ABBREVIATIONS AND SYMBOLS

AMD	: Adiabatic Matching Device
BPM	: Beam Position Monitor
CDR	: Conceptual Design Reports
CERN	: The European Organisation for Nuclear Research
CLIC	: Compact Linear Collider
ILC	: International Linear Collider
LEP	: Large Electron-Positron Collider
LHC	: Large Hadron Collider
Linac	: Linear Accelerator
PEDD	: Peak Energy Deposition Density
PLACET	: Program for Linear Accelerator Correction Efficiency Tests
RF	: Radiofrequency
SLAC	: Stanford Linear Accelerator Center
TAEK	: Turkish Atomic Energy Authority
TBA	: Two-Beam Acceleration

ACKNOWLEDGEMENTS

I would like to express appreciation to my supervisor, Prof. Dr. Haluk Denizli, always trust and help me with his knowledge, guidance and moral support to finish my research. I also thank him for tolerance and kindness.

I would like to thanks my co-supervisors who are Dr. Daniel Schulte and Dr. Andrea Latina for their guidance and unimaginable knowledge they taught me about accelerator physics during my stay at CERN.

I would like to special thanks my friends who are Kaan Yüksel Oyulmaz, Sinan Öztel and Özgün Karadeniz for their friendships, supports and suggestions.

The author also would like to thank Turkish Atomic Energy Authority (TAEK) for supporting this thesis work under the project number 2013TAEKCERN-A5.H2.P1.01-24.

I am grateful to my father, mother and my sister for their support, patiance and financial support from begining to end.

1. INTRODUCTION

Researches for particle interactions at the terascale are considered to hide the answers of many key questions in particle physics. Understanding phenomena such as Dark Matter and physics Beyond the Standard Model may be possible with the LHC (Large Hadron Collider) which brought experimental access to Terascale physics. With the future LHC luminosity and development of new high energy accelerators will also increase possibility to find detailed answers to these questions. On the other hand, results of the LHC need to be complemented and backed by experiments with a lepton collider in the tera-electron-volt (TeV) energy scale.

For the LHC tunnel, highest energy lepton collisions were at 209 GeV which have been reached by LEP (Large Electron-Positron Collider) at CERN. There are some restrictions and limitations in this situation for the 27 km circumference of LEP. One of them is synchrotron radiation losses by a superconducting RF system which providing 3640 MV per revolution. Here, synchrotron radiation is inversely proportional to the bending radius and proportional to the fourth power of the particle mass. Hence, there are two alternatives to overcome this limitation and build a Terascale lepton collider:

- Use muons which have a mass 207 times larger than electrons.
- Use e^+ e^- linear colliders which consist of two opposing linear accelerators and they accelerate the particles to their final energy and colliding them in a central interaction point (IP).

In SLAC Linear Collider (SLC) (SLAC Linear Collider (SLC), 2001), 25 years of R&D and progress improved working performances of linear colliders. Also, two global collaborations are working on different technologies for linear colliders with different energy ranges. One of them is International Linear Collider (ILC) (International Linear Collider, 2013) which has colliding beam energy up to 500 GeV and upgradable to 1 TeV and it provides beam acceleration by using superconducting RF cavities. The other one is the Compact Linear Collider (CLIC) which is focusing on extending energy scale of linear colliders into the multi-TeV scale with a new technology of two-beam acceleration (TBA). This technology will provide colliding beams up to 3 TeV.

1.1 Linear Accelerators

The term linear accelerator may be expected to refer any device that accelerates particles through a straight line. However, linear accelerator (linac) term stands for an accelerator that charged particles move on a linear track and are accelerated by time-dependent electromagnetic fields. In the case of an RF (radiofrequency) linac, the beam is accelerated by using radio-frequency electromagnetic fields with a harmonic time dependence (Wangler, 1998, Chapter 1).

A main advantage of the linear accelerator is its ability for providing charged particle beams of high beam quality with high-energy and high-intensity. High beam quality term can be related to a capacity for producing a beam with small diameter and small energy spread. Other useful characteristic of linacs are;

- Strong focusing can easily be provided.
- There is no power loss from synchrotron radiation which is restriction for high-energy electron beams in circular accelerators, because the beam is travelling in a straight path.
- Beam injection and extraction is easier than the circular accelerators, since the natural trajectory of the linac is open at the both end of the linac; special techniques for effective beam injection and extraction are redundant.
- The linac can operate at higher duty factors like 100% or a continuous wave that outcomes in acceleration of charged-particle beams with higher average current.

1.1.1 Linac Structures

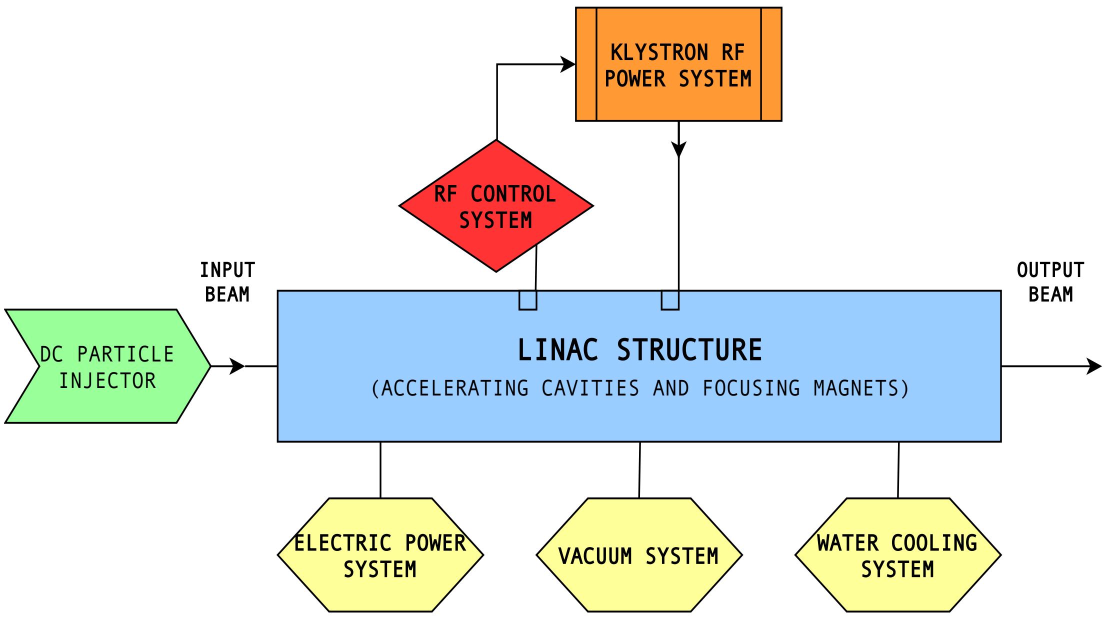

Figure 1.1. Simplified block diagram of a linac.

Components of a linac is demonstrated in Figure 1.1. In a linac, linac structure consists of accelerating cavities and focusing-defocusing magnets. Electromagnetic energy needed for linac structures is supplied by an RF power system which uses electric power primarily. Beam is injected inside linac structure from a DC particle injector system. For providing a fine beam transmission, a vacuum system is necessary. When injected beam is traveling through linac structures, heat is generated from resistive walls. Therefore, it must be cooled with a water cooling system. The water cooling system lowers the heat for normal-conducting linac structures, but for linacs with superconducting structures, a liquid helium cooling system is required (Wangler, 1998, Chapter 1).

Since the linear accelerator uses an electric field for acceleration which is sinusoidally diversifying, particles may either lose or gain energy depending on the beam phase. Therefore, to provide influential acceleration for all the charged particles in a beam, the beam must be bunched.

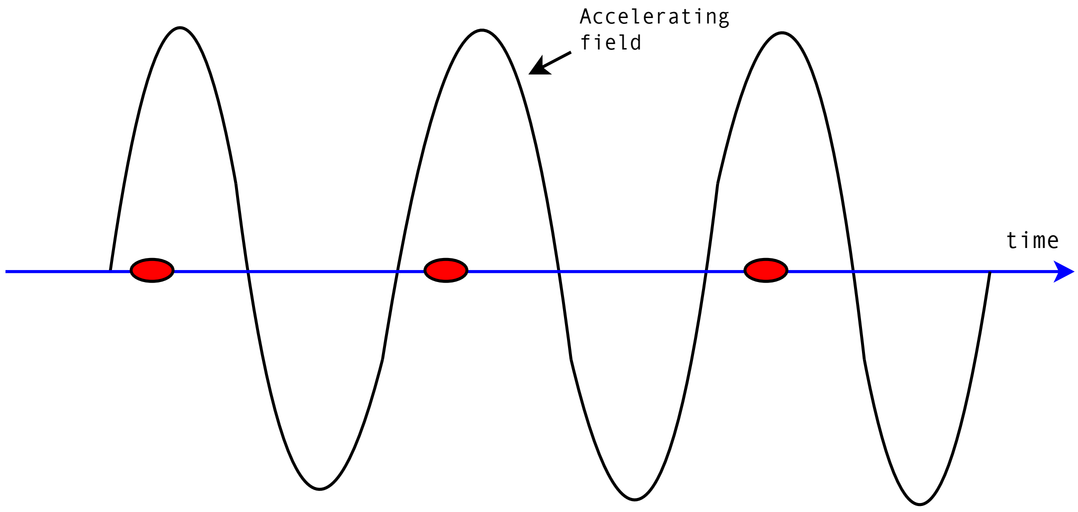

Figure 1.2. Representation of beam bunches in an RF linac.

As in Figure 1.2, the bunches might be separated longitidunally by one or more RF periods.

1.2 Particle Beam Guidance

If a charged particle with velocity $\vec{v}$ moves under effect of magnetic field, there will be a force affecting the particle beam.

$$\vec{F} = e\,[\vec{v} \times \vec{B}] + e\vec{E} \tag{1.1}$$

Lorentz force has two components related to $\vec{E}$ and $\vec{B}$, which are the electrical and magnetic field vectors respectively, but beam bending and focusing can only be done with magnetic fields.

When an orthogonal force has an effect upon a particle's velocity vector, particle makes centrifugal movement. The force on a particle that moves in a centripetal orbit is;

$$F = \frac{m\, v^2}{\rho} \qquad (1.2)$$

where ρ stands as bending radius. One can define the particle's movement due to equilibrium of centrifugal force and Lorentz force

$$\frac{\gamma m v^2}{\rho}\vec{n} + e\,[\,\vec{v} \times \vec{B}] = 0. \qquad (1.3)$$

Here, $\vec{n}$ is the unit vector in the direction of centrifugal force and γ is relativistic Lorentz factor (Wiedemann, 2015, Chapter 5).

The beam rigidity Bρ is given

$$B\rho\ [T.m] = \frac{pc}{ec} = \frac{\beta E}{ec} = \frac{\gamma\beta E_o}{ec} = \frac{10}{2.998}\beta E\ [\mathrm{GeV}] \qquad (1.4)$$

When bending radius ρ is constant, high intensity magnetic fields are required for keeping higher velocity particles in a track.

1.3 Phase Space Transformation, Beam Emittance and Twiss Parameters

At the beginning of a beamline, the information of an area in phase space which occupied by the particles will allow us to specify distribution and location of the beam at any other space throughout the beamline without doing any calculation about trajectory of every single particle.

In most beam dynamics calculations, the space density by using trajectory slopes instead of tansverse momenta (only as long as p_0 is constant) is a true choice. Thus, we have two definitions of the beam emittance which is the area in phase space that the particles in a beam take up.

$$\epsilon_n = \beta\gamma\epsilon, \tag{1.5}$$

Here, ϵ_n is the normalized emittance that depends on space-momentum phase space and ϵ is the geometric emittance based upon space-slope phase space. Also, where $\beta = v/c$ is the relative particle velocity as well as γ is the relativistic factor.

The definition of phase ellipse in beam dynamics is the ellipse that surrounds all particles of a beam in phase space as shown in Figure 1.3. The phase ellipse is described by

$$\gamma x^2 + 2\alpha x x' + \beta x'^2 = \epsilon, \tag{1.6}$$

where ellipse parameters are α, β, γ and ϵ. Here, ϵ is the geometric beam emittance which is described as area surrounded by the ellipse

$$\int_{ellipse} dx\, dx' = \pi\epsilon, \tag{1.7}$$

since the parameters α, β and γ specify the direction and shape of the ellipse.

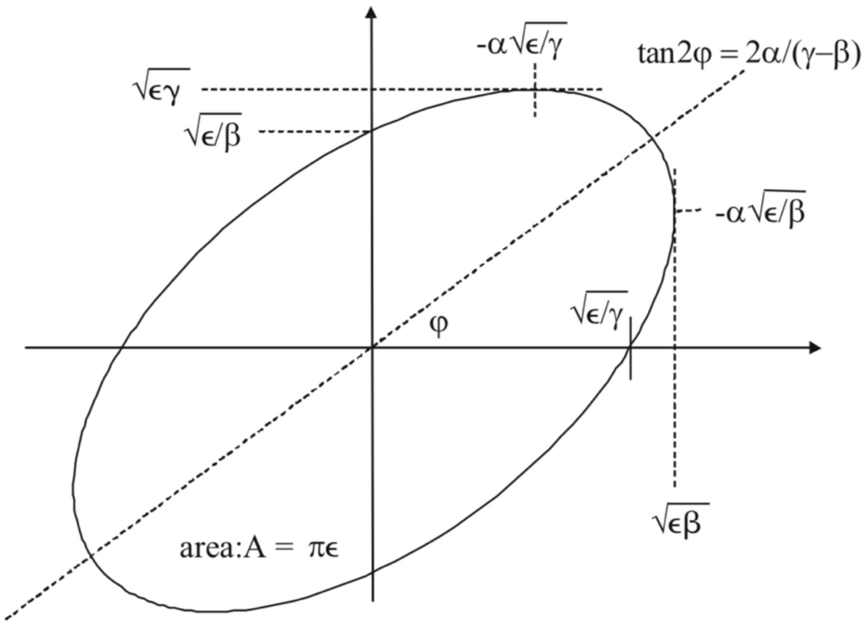

Figure 1.3. Representation of phase space ellipse (Wiedemann, 2015, p. 219).

Consequently, for describing the whole particle beam, we only need to know how the ellipse parameters transform along the beamline.

$$\gamma_0 x_0^2 + 2\alpha_0 x_0 x_0' + \beta_0 x_0'^2 = \epsilon \tag{1.8}$$

From the starting point $z = 0$ of the beamline, let the Equation (1.8) to be the equation of the phase ellipse, then from the starting point $z = 0$ to any other point $z \neq 0$ every single particle trajectory will transform by the transformation $\begin{pmatrix} x(z) \\ x'(z) \end{pmatrix} = \begin{pmatrix} C(z) & S(z) \\ C'(z) & S'(z) \end{pmatrix} \begin{pmatrix} x_0 \\ x_0' \end{pmatrix}$. Solving for x^0 and x_0' and put the results in Equation (1.8), and after sorting parameters we get an equation without (z)-dependence

$$\begin{aligned} \epsilon = (C'^2\beta_0 - 2\,S'C'\alpha_0 + S'^2\gamma_0)x^2 \\ + 2(-CC'\beta_0 + S'C\alpha_0 - SS'\gamma_0)xx' \\ +(C^2\beta_0 - 2\,S\,C\alpha_0 + S'\gamma_0)x'^2. \end{aligned} \tag{1.9}$$

This Equation (1.9) can be shaped into the form of the Equation (1.6) by replacing the coefficients with

$$\gamma = C'^2\beta_0 - 2S'C'\alpha_0 + S'^2\gamma_0,$$
$$\alpha = -CC'\beta_0 + (S'C + SC')\alpha_0 + S\,S'\gamma_0, \quad (1.10)$$
$$\beta = C^2\beta_0 - 2SC\alpha_0 + S^2\gamma_0.$$

The Equation (1.10) is the resulting ellipse equation and according to its different parameters γ, α, β, it has a distinctive shape and orientation. If a transformation is considered along a beam transport line, one can easily determine the phase ellipse will change its shape and direction but most importantly not its area. In matrix representation of these ellipse parameters, which are also called Twiss parameters (Twiss and Frank, 1949), can be transformed from Equation (1.10) as

$$\begin{pmatrix} \beta(z) \\ \alpha(z) \\ \gamma(z) \end{pmatrix} = \begin{pmatrix} C^2 & -2CS & S^2 \\ -CC' & CS' + C'S & -SS' \\ C'^2 & -2C'S' & S'^2 \end{pmatrix} \begin{pmatrix} \beta_0 \\ \alpha_0 \\ \gamma_0 \end{pmatrix}. \quad (1.11)$$

1.4 FODO Lattice

In an accelerator, especially in circular machines, lattice cells can be FODO, Double Bend Achromat (DBA), Triple Bend Achromat (TBA), Quadruple Bend Achromat (QBA) or Multi-Bend Achromat (MBA) types. The FODO lattice is the most common used lattice exclusively in high energy accelerators due to its benefits such as simplicity, beam dynamical stability and providing most space for bending magnets compared to the other lattice types.

The simplest way to create a FODO cell is shown in Figure 1.4, in which each cell of a FODO lattice consists of a sequence of focusing quadrupoles with equal distant and strength. Each half period of a FODO cell created with a focusing (F) and a defocusing (D) quadrupole with equally set drift space (O) between them generating a FODO sequence.

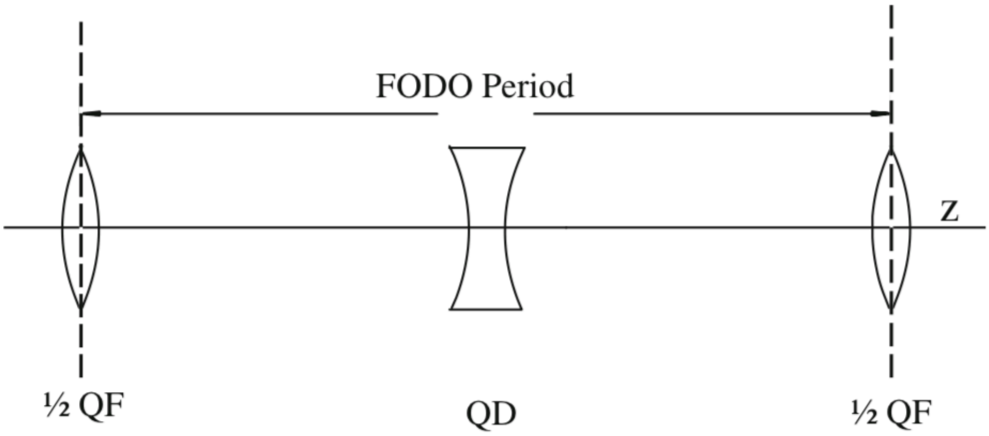

Figure 1.4. FODO-lattice (QF focusing quadrupole, QD defocusing quadrupole) (Wiedemann, 2015, p. 304).

1.4.1 Transfer Matrix of FODO Lattice

By using thin lens approximation method, we can determine the specifications and stability criteria for a FODO cell. Transfer matrices for focusing and defocusing quadrople magnets are

$$M_{Q_{Defocusing}} = \begin{pmatrix} 1 & 0 \\ K & 1 \end{pmatrix} \tag{1.12}$$

$$M_{Q_{Focusing}} = \begin{pmatrix} 1 & 0 \\ -K & 1 \end{pmatrix} \tag{1.13}$$

$$M_{O(Drift)} = \begin{pmatrix} 1 & L \\ 0 & 1 \end{pmatrix} \tag{1.14}$$

where K is $1/f$ and which is focal length of the quadrupole. Thus, the transfer matrix from center of one focusing quadrupole to the center of other focusing quadrupole can be calculated by multiplication of matrices as follows.

$$M_{FODO} = M_{Q_{F/2}}.M_O.M_{Q_D}.M_O.M_{Q_{F//2}} \tag{1.15}$$

$$M_{FODO} = \begin{pmatrix} 1 & 0 \\ -K/2 & 1 \end{pmatrix} \begin{pmatrix} 1 & L \\ 0 & 1 \end{pmatrix} \begin{pmatrix} 1 & 0 \\ K & 1 \end{pmatrix} \begin{pmatrix} 1 & L \\ 0 & 1 \end{pmatrix} \begin{pmatrix} 1 & 0 \\ -K/2 & 1 \end{pmatrix} \tag{1.16}$$

$$M_{FODO} = \begin{pmatrix} 1 & 0 \\ -K/2 & 1 \end{pmatrix} \begin{pmatrix} 1 & L \\ 0 & 1 \end{pmatrix} \begin{pmatrix} 1 & 0 \\ K & 1 \end{pmatrix} \begin{pmatrix} 1-KL/2 & L \\ -K/2 & 1 \end{pmatrix} \tag{1.17}$$

$$M_{FODO} = \begin{pmatrix} 1 & 0 \\ -K/2 & 1 \end{pmatrix} \begin{pmatrix} 1 & L \\ 0 & 1 \end{pmatrix} \begin{pmatrix} 1-KL/2 & L \\ K/2\,(1-KL) & 1+KL \end{pmatrix} \tag{1.18}$$

$$M_{FODO} = \begin{pmatrix} 1 & 0 \\ -K/2 & 1 \end{pmatrix} \begin{pmatrix} 1-K^2L^2/2 & L\,(2+KL) \\ K/2\,(1-KL) & 1+KL \end{pmatrix} \tag{1.19}$$

$$M_{FODO} = \begin{pmatrix} 1-K^2L^2/2 & L\,(2+KL) \\ -K^2L/2\,(1-KL/2) & 1-K^2\,L^2/2 \end{pmatrix} \tag{1.20}$$

changing K as $1/f$ and -K as -$1/f$, transfer matrix becomes

$$M_{FODO} = \begin{pmatrix} 1-L^2/2f^2 & L\,(2+L/f) \\ -L/(\,2f^2(1-L/2f)) & 1-L^2/(2f^2) \end{pmatrix} \tag{1.21}$$

1.4.2 Scaling of FODO Parameters

The diagonal elements in matrix form are equal in any symmetric lattice. When one compares this property by using the transformation matrix represented in terms of betatron functions given in Equation (1.22).

$$\begin{pmatrix} C(z) & S(z) \\ C'(z) & S'(z) \end{pmatrix} = \begin{pmatrix} \sqrt{\frac{\beta}{\beta_0}}(\cos\psi + \alpha_0 \sin\psi) & \sqrt{\beta\beta_0}\sin\psi \\ \frac{\alpha_0-\alpha}{\sqrt{\beta\beta_0}}\cos\psi - \frac{1+\alpha\alpha_0}{\sqrt{\beta\beta_0}}\sin\psi & \sqrt{\frac{\beta_0}{\beta}}(\cos\psi - \alpha\sin\psi) \end{pmatrix} \tag{1.22}$$

It shows that the betatron function is periodic and symmetric according to its solution since $\alpha = 0$ both at the end and the beginning of the lattice period. This leads symmetry planes for betatron functions in the middle of the quadrupole magnets for both vertical and horizontal planes. This symmetric form of betatron function is shown in Figure 1.5.

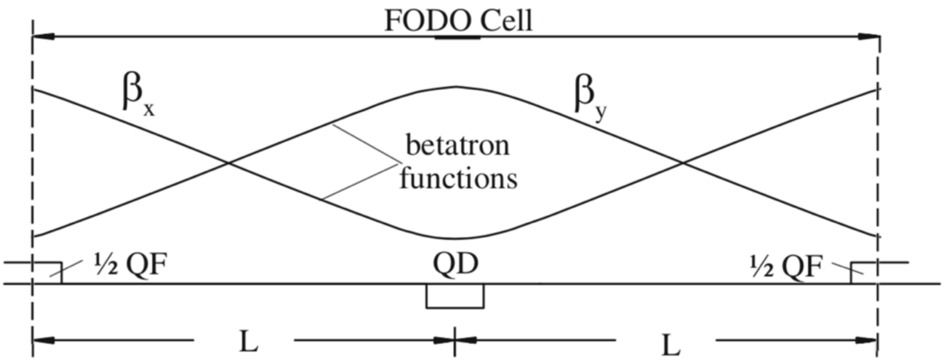

Figure 1.5. Periodic betatron functions in a FODO lattice (Wiedemann, 2015, p. 305).

The analytical expression for the symmetric and periodic betatron functions can be determined by using Twiss parameters in Equation (1.10). Setting $\beta_0 = \beta$, $\alpha_0 = 0$ and $\gamma_0 = 1/\beta$;

$$\beta = \left(1 - 2\frac{L^2}{f^2}\right)^2 \beta + 4L^2 \left(1 + \frac{L}{f}\right)^2 \frac{1}{\beta}. \tag{1.23}$$

Now, we can derive betatron function in the middle of the focusing and defocusing quadrupole by solving Equation (1.23) for β. Resulting equations are shown in the Equations (1.24) and (1.25);

$$\beta^+ = L\frac{\frac{f}{L}\frac{f}{L+1}}{\sqrt{\frac{f^2}{L^2-1}}} = L\frac{K(K+1)}{\sqrt{K^2-1}} \tag{1.24}$$

$$\beta^- = L\frac{K(K-1)}{\sqrt{K^2-1}} \tag{1.25}$$

where K is the FODO parameter and defined as;

$$K = \frac{f}{L} > 1 \tag{1.26}$$

The betatron phase for a FODO cell can be derived by applying Equation (1.22) to a symmetric lattice ($\alpha_0 = \alpha = 0$ and $\beta_0 = \beta$);

$$\begin{pmatrix} \cos\phi & \beta\sin\phi \\ -\frac{1}{\beta}\sin\phi & \cos\phi \end{pmatrix} \tag{1.27}$$

where ϕ is the betatron phase advance along a full symmetric period. Since matrix in the Equation (1.21) must be equal to matrix in Equation (1.27), and the phase becomes

$$\cos\phi = 1 - 2\frac{L^2}{f^2} = \frac{K^2-2}{K^2} \tag{1.28}$$

or can be evaluated from

$$\sin\frac{\phi}{2} = \frac{1}{K}\,. \tag{1.29}$$

The condition in Equation (1.29) points out that the distance from half a quadrupole to the other quadrupole must be shorter than the focal length of half a quadrupole. In addition, the quadrupole strengths have a critical role on the periodic betatron function solutions. Here, one can take $d\beta^+/dK = 0$ and rewrite Equation (1.24) as

$$K_0^2 - K_0 - 1 = 0 \tag{1.30}$$

and solve to get roots as follows

$$K_0 = \frac{1}{2} \pm \sqrt{\frac{1}{4} + 1} = 1.6180. \tag{1.31}$$

Therefore, one can deduce that the phase advance per FODO cell;

$$\phi_0 \approx 76.345°. \tag{1.32}$$

When phase advance is about 76.3° per cell, this means the maximum betatron function attains a minimum for a FODO lattice.

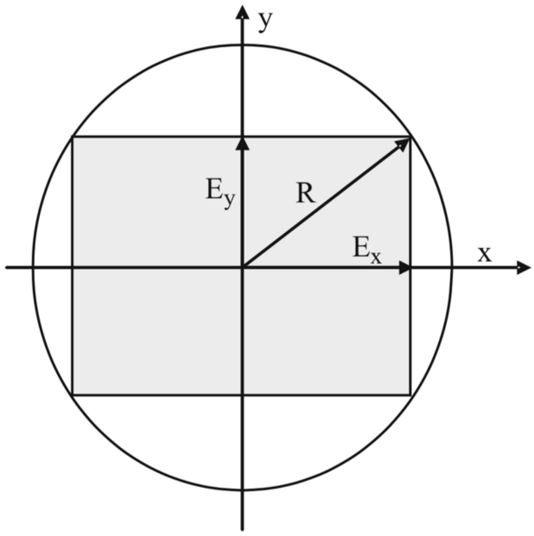

Figure 1.6. Maximum beam acceptance of a FODO lattice with a circular aperture of radius R and where $\boldsymbol{E_{x,y}} = \sqrt{\boldsymbol{\epsilon_{x,y}\beta_{x,y}}}$ (Wiedemann, 2015, p. 308).

As shown in Figure 1.6, for reaching the maximum beam acceptance for a FODO, the beam diameter must be minimized. The aperture radius $R^2 = E_x^2 + E_y^2 \sim \beta_x + \beta_y$ can be written in terms of beam envelopes E_x and E_y in the horizontal and vertical planes, respectively. This minimum of beam diameter is determined by setting $d(\beta_x + \beta_y)/dK = 0$ that leads to

$$K_{opt} = \sqrt{2}\,. \tag{1.33}$$

From Equation (1.29), the optimum betatron phase per cell is

$$\phi_{opt} = 90°. \tag{1.34}$$

By considering equal beam emittances in both x and y planes $\epsilon_x = \epsilon_y = \epsilon$ with a minimum radial aperture R in quadrupole magnets for a beam, the betatron functions in middle of quadrupoles can be simplified as;

$$\beta_{opt}^{+} = L(2 + \sqrt{2}),$$
$$\beta_{opt}^{-} = L(2 - \sqrt{2}). \tag{1.35}$$

By using Equation (1.35) one can find $(\beta^{+}+\beta^{-})_{opt} = 4L$, and maximum beam acceptance of a FODO with an aperture of radius R is

$$\epsilon_{max} = \frac{R^2}{4L}. \tag{1.36}$$

1.5 Quadrupole Magnets

Quadrupole magnets are the magnets with four poles and used for focusing a particle beam horizontally or vertically.

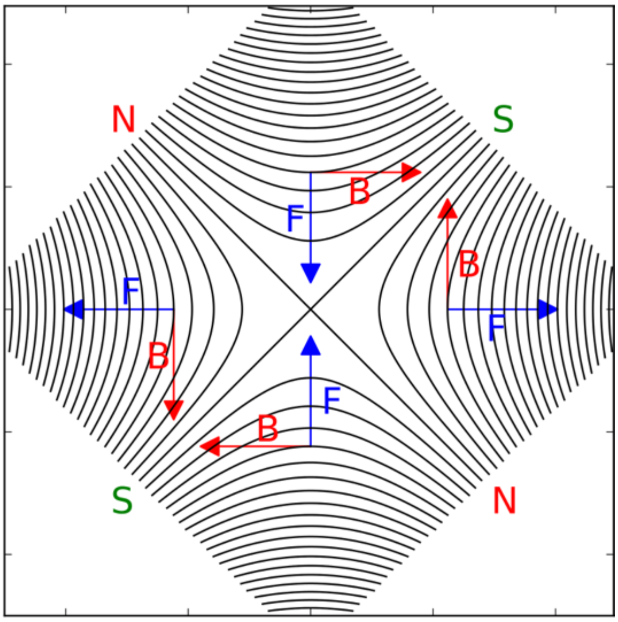

Figure 1.7. Demonstration of magnetic field and Lorentz forces in a quadrupole magnet.

In Figure 1.7, red arrows show the direction of the magnetic field and the blue arrows show the direction of the Lorentz force. The magnetic field of a quadrupole is proportionally increased with the distance of axis. With this setup, the quadrupole is focusing a positive particle travelling into the image plane which is away from the page. Furthermore, the focusing strength of a quadrupole *k* can be shown as

$$k = \frac{1}{(B\rho)}\frac{dB_y}{dx} = \frac{g}{B.\rho} \quad [\mathrm{m}^{-2}] \tag{1.37}$$

where g is the gradient of the magnetic field and given as

$$g = \frac{2\mu_0 nI}{r^2} \quad [\text{T/m}] \,. \tag{1.38}$$

Also, the focal length of a quadrupole magnet is

$$f = \frac{1}{k.L} \; [\text{m}] \tag{1.39}$$

which is demonstrated in Figure 1.8. Focal length can be determined as a function of distance between the lens and focal point which parallel beam rays focused to a point.

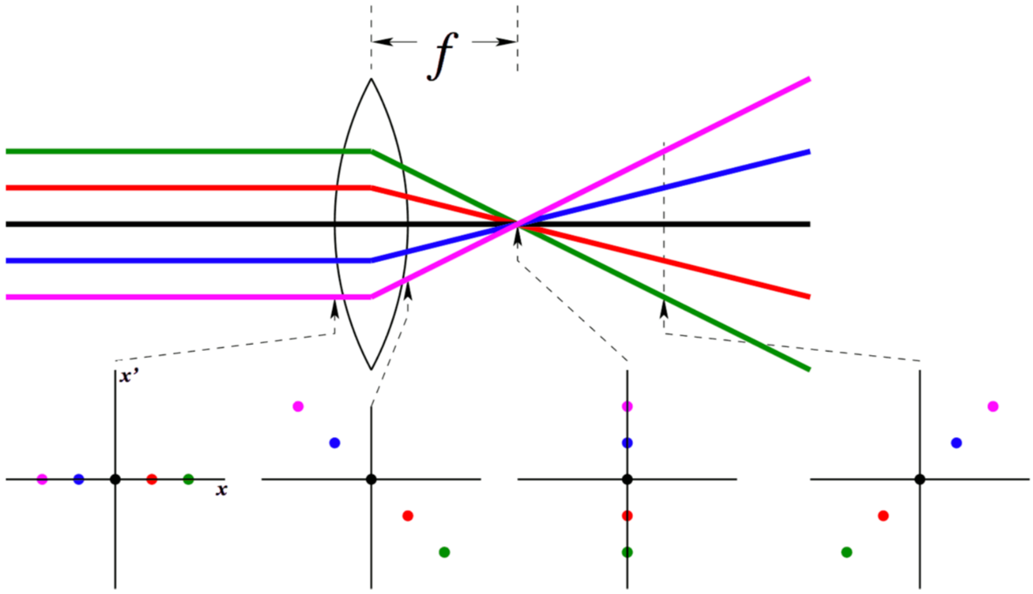

Figure 1.8. Representation of principle of focusing.

1.5.1 Transfer Matrix of a Quadrupole Magnet

A quadrupole in focusing plane is defined by

$$x'' + kx = x'' + |k|x = 0 \tag{1.40}$$

$$M_{Q_F} = \begin{pmatrix} \cos(\sqrt{k}L) & \frac{1}{\sqrt{k}}\sin(\sqrt{k}L) \\ -\sqrt{k}\sin(\sqrt{k}L) & \cos(\sqrt{k}L) \end{pmatrix}, \tag{1.41}$$

and a quadrupole in defocusing plane is defined by

$$x'' + kx = x'' - |k|x = 0 \tag{1.42}$$

$$M_{Q_D} = \begin{pmatrix} \cosh\left(\sqrt{|k|}L\right) & \frac{1}{\sqrt{|k|}}\sinh\left(\sqrt{|k|}L\right) \\ -\sqrt{|k|}\sinh\left(\sqrt{|k|}L\right) & \cosh\left(\sqrt{|k|}L\right) \end{pmatrix}. \tag{1.43}$$

If we assume that is a thin lens quadrupole and using thin lens approximation method, one can calculate the matrix representation of focusing and defcosuing quadrupoles as ($L\rightarrow 0$, $kL = K = 1/f$);

$$M_{Q_F} = \begin{pmatrix} 1 & 0 \\ -K & 1 \end{pmatrix}, \qquad M_{Q_D} = \begin{pmatrix} 1 & 0 \\ K & 1 \end{pmatrix} \tag{1.44}$$

1.6 Dipole Magnets

Dipole magnets are used for bending the beam trajectory that moves along a straight path. Between dipole's two poles, a homogenous magnetic field B_0 is generated as shown in Figure 1.9;

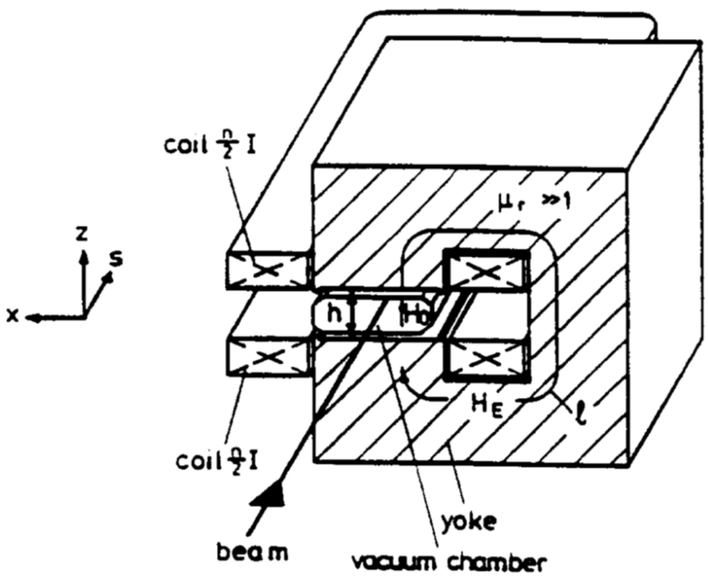

Figure 1.9. Schematic view of a dipole magnet (Rossbach and Schmüser, 1992, p. 22).

The magnetic field is calculated as follows;

$$\oint H \cdot ds = hH_0 + \ell H_E = n\, I$$

$$H_E = \frac{1}{\mu_r} \cdot H_0 \qquad (1.45)$$

For $\mu_r \gg 1$;

$$B_0 = \frac{\mu_0 n I}{h} \qquad \text{h = gap height} \qquad (1.46)$$

Equation (1.46) is only an approximation. Thus, one can calculate the radius of curvature (bending strength) for a particle of charge ***e*** and momentum ***p***;

$$\frac{1}{\rho}[\mathrm{m}^{-1}] = \frac{eB_0}{p} = \frac{B_0[\mathrm{T}]}{[\mathrm{GeV/c}]} \qquad (1.47)$$

1.6.1 Transfer Matrix of a Dipole Magnet

Dipole magnets can be classified by geometrical shapes such as sector, wedge or rectangular. If it has two parallel end faces, we can call this wedge dipole magnet as rectangular dipole magnet. If we install a rectangular dipole magnet about the planned particle trajectory, the exit and the entrance angles will be equal to half the bending angle as shown in Figure 1.10.

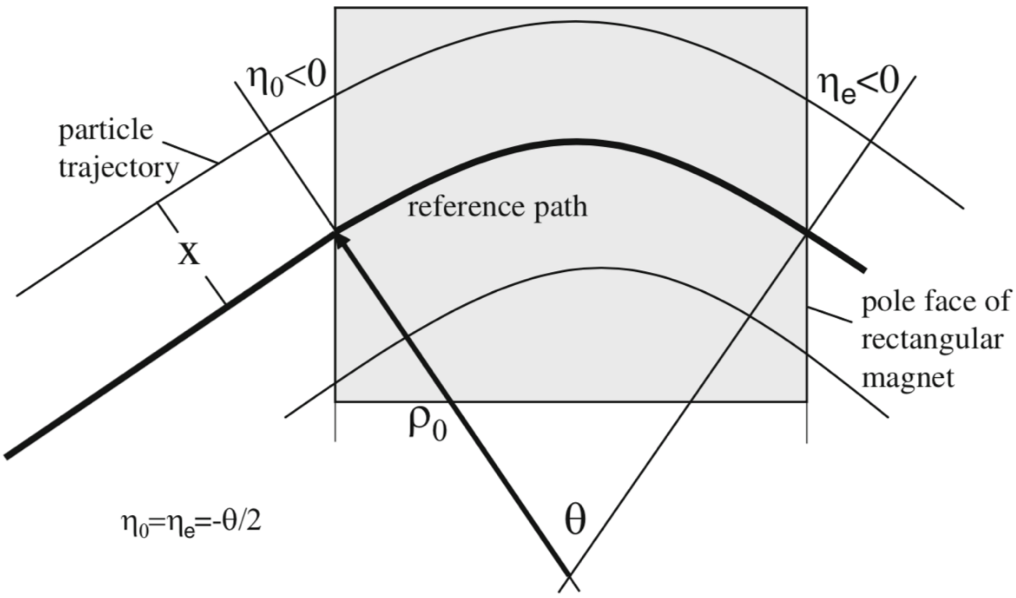

Figure 1.10. Rectangular dipole magnet (Wiedemann, 2015, p. 199).

Rectangular dipole magnets are commonly used since their shapes are easier to design. Thus, we can only write transfer matrix for rectangular shaped dipole magnet to conclude transfer matrices. So, for a deflection angle θ like in Figure 1.10, $\eta_0 = \eta_e = -\theta/2$ where η_0 and η_e arbitrary entrance and exit angles. Transfer matrix in this deflecting plane is;

$$M_{r,p}(\ell \mid 0) = \begin{pmatrix} 1 & 0 \\ -\frac{\tan \eta_e}{\rho_0} & 1 \end{pmatrix} \begin{pmatrix} \cos\theta & \rho_0 \sin\theta \\ -\frac{\sin\theta}{\rho_0} & \cos\theta \end{pmatrix} \begin{pmatrix} 1 & 0 \\ -\frac{\tan \eta_0}{\rho_0} & 1 \end{pmatrix}$$

$$= \begin{pmatrix} 1 & \rho_0 \sin\theta \\ 0 & 1 \end{pmatrix}. \quad (1.48)$$

A rectangular dipole magnet does not focus the beam and transforms in the deflecting plane like a drift space of length $\rho_0 \sin\theta$. ℓ is the magnet length defined by the deflection angle $\theta = \ell/\rho_0$ is the arc length and associated with the straight magnet length L by

$$L = 2\rho_0 \sin\frac{\theta}{2} = 2\rho_0 \sin\frac{\ell}{2\rho_0} \cdot \tag{1.49}$$

Focusing with focal length in the vertical plane can be described as

$$\frac{1}{f_y} = +\frac{1}{\rho_0}\left(\tan\frac{\theta}{2} - \frac{\delta_{\theta/2}}{3}\right) \cdot \tag{1.50}$$

Inserting $\delta_{\theta/2} = G/[\rho_0 \cos(\theta/2)]$ and $\delta_{\theta/2} = 2G \tan(\theta/2)\, L$ from Equation (1.49) into Equation (1.50), and the transfer matrix of a rectangular dipole (bending) magnet in the nondeflecting plane

$$M_{r,0}(\ell \mid 0) = \begin{pmatrix} 1 & 0 \\ -\frac{1}{f_y} & 1 \end{pmatrix} \begin{pmatrix} 1 & \ell \\ 0 & 1 \end{pmatrix} \begin{pmatrix} 1 & 0 \\ -\frac{1}{f_y} & 1 \end{pmatrix} = \begin{pmatrix} 1 - \frac{\ell}{f_y} & \ell \\ -\frac{2}{f_y} + \frac{\ell}{f_y^2} & 1 - \frac{\ell}{f_y} \end{pmatrix} \cdot \tag{1.51}$$

where

$$\frac{1}{f_y} = \frac{1}{\rho_0}\left(1 - \frac{2G}{3L\cos(\theta/2)}\right) \tan\left(\frac{\theta}{2}\right) \cdot \tag{1.52}$$

From (1.52), one can see that the focusing strength is reduced by the fraction $2G/[3L\cos(\theta/2)]$ where the term L is the straight magnet length and *2G* is the gap height of the rectangular dipole magnet.

1.7 Beam Instabilities

1.7.1 Short-Range and Long-Range Wakefields

There are interactions between the electrons in a bunch and the linac structure if an electron bunch moves along a periodic linac structure. These interactions will cause changes in beam energies of electrons in same bunch. Generally, the fields that carried together with the bunch cause currents and surface charges in the walls of linac structure, and these grow into sources of fields itselves which act back on the particles in the bunch.

When the fields moving with the relativistic particles encounter different geometric shape variations inside the linac structure such as RF cavities, scattered electromagnetic radiation is produced. If extreme relativistic limit scenario is considered, the scattered radiation cannot catch up to affect the particles from source but the radiation can catch and does act on the particles that trailing other ones in the same or later bunches. Here, the scattered radiation will be called wakefields, although exactly speaking, for particles with $v < c$, the scattered radiation does not always chase behind the particles that are its source (Wangler, 1998, Chapter 11).

These radiated fields are sometimes categorised as either short-range or long-range wakefields. Short-range wakefields are generated by the particles at the beginning of the bunch affect the particles that following other particles in the same bunch, causing energy loss and for bunches which are off-axis will deflect the particles in the tail of the bunch transversely. On the other hand, long-range wakefields are caused by the transverse deflecting modes that bring about time-dependent transverse deflections in the bunches which trailing. Here, a beam-breakup instability which leading to emittance growth may occur if the deflecting modes are vigorously excited by the beam. In the end, the beam is lost on the walls (Wangler, 1998, Chapter 11).

2. AIM AND SCOPE OF THE STUDY

Accelerators are the tools to accelerate charged particles through a created medium. Since an accelerator is a complex machine and one of the costliness machines in the world, design of each structure and optimization of each parameter are very important in an accelerator facility. CLIC (Compact Linear Collider) will be the future linear collider designed to collide electron-positron beams with a center of mass energies up to 3 TeV. Creating electrons and positrons are done in one of the most important parts of CLIC which is the main beam injector complex. Here, positrons are produced by impinging electrons on a tungsten target. In the main beam injector complex, these electrons are accelerated up to 5 GeV in an electron linac as described in CLIC-Conceptual Design Report (CLIC-CDR). The necessary parameters for this work was given in CLIC-CDR, but the preliminary design for this linac was not done. Thus, the main goal of this thesis to design a 5 GeV electron linac and study beam dynamics with PLACET (Program for Linear Accelerator Correction Efficiency Tests) program. Moreover, since this linac will be the most power consuming machine in the main beam injector complex due to its higher beam current. Optimization of this linac will also be done in this thesis.

3. MATERIALS AND METHODS

3.1 A Multi-TeV Linear Collider Based on CLIC Technology

The CLIC is considered to be a linear collider at the multi-TeV scale and can offer new physics discoveries and precision measurements, and will be perfectly complementing the LHC. Furthermore, the two-beam acceleration idea which is proposed in 1986 provides a unique approach to reach multi-TeV energies with an $e^+ e^-$ collider. The CLIC concept has been studied and developed in 1990s but in 2004, by the CERN Council's decision, the Conceptual Design Report (CDR) published in 2012 (CLIC Conceptual Design Report, 2012, Chapter 1).

As an international collaboration, the CLIC has 44 partners in 22 countries. Also, the CLIC is hosted by CERN and the CLIC test facility at CERN remains as the main part of the CLIC project. For CLIC study, Conceptional Design Reports for both accelerator studies as well as the detector and physics studies were published. Both accelerator and physics/detector studies in these CDR volumes have primarily focused on the 3 TeV implementation of the CLIC. Reports also include studies for initial 500 GeV machine which is considered to be rearranged with a rebaseline study to 380 GeV in new studies (CLIC Conceptual Design Report, 2012, Chapter 1).

3.2 CLIC Main Beam Injector Complex

The CLIC Main Beam injector complex consist of a polarized electron source and a positron source. In this part of the study, electrons and positrons are pre-accelerated up to 200 MeV before they are injected into a common injector linac which brings the energy scale up to 2.86 GeV for the pre-damping and damping ring complex. For the whole complex, the RF frequency is chosen about 2 GHz, although the bunch spacing before damping ring complex is only 1 GHz. Consequently, this choice gives a way to reach high accelerating gradient and the possibility to use the same RF system throughout the whole injector complex.

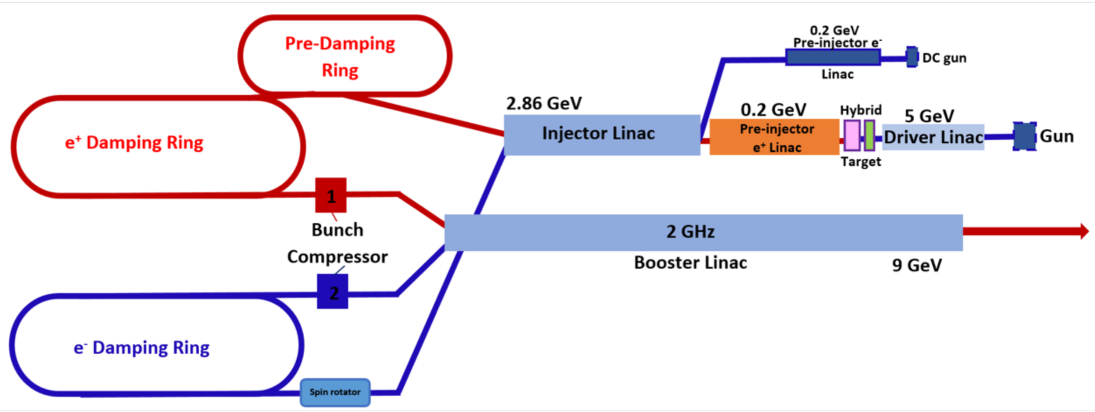

Figure 3.1. Schematic layout of the Main Beam injector complex (Bayar et al., 2017).

In Figure 3.1, a schematic layout of the CLIC Main Beam injector complex is shown up to the pre-damping rings. The Main Beam injector complex consists of a polarized electron source with its pre-injector, a 5 GeV drive linac, two positron conversion targets followed by pre-injectors, and a common injector linac which accelerates both particle species up to 2.86 GeV. The 2 GHz linac technology is a commonly used technology for many years in major accelerators labs. Also, the polarized electron source uses challenging technologies like ultra-high vacuum system, thin-film cathodes and a high-power laser and its design concept is based on systems already used in existing facilities throughout the world. Moreover, the most challenging part in the Main Beam injector is the target for positron production and capturing the positrons that produced from it, and transferring positrons with large emittance to the damping rings (CLIC Conceptual Design Report, 2012, Chapter 3).

3.2.1 5 GeV Driver Linac for e^+ in the CLIC Main Beam Injector Complex

The driver linac in the CLIC Main Beam injector complex is a e^- linac and considered to accelerate electrons up to 5 GeV. Electrons with energy of 50 MeV from an electron are accelerated up to 5 GeV at the very end of this linac. This primary 5 GeV electron linac followed by hybrid targets (one thin crystal tungsten target and one thick amorphous tungsten target), a positron capture section for capturing them after producing process of positrons and a pre-injector linac to accelerate captured positrons to 200 MeV. The 5 GeV electron beam which is oriented on its ⟨111⟩ axis and generates a photon beam with a large population of soft photons. The characteristics of the electron beam impinging on the crystal target are summarized in the Table 3.1 (CLIC Conceptual Design Report, 2012, Chapter 3).

Table 3.1. Primary electron beam parameters (CLIC Conceptual Design Report, 2012, p. 103).

Parameter	Value
Energy [GeV]	5
Number of e^- / bunch	1.1×10^{10}
Charge per bunch [nC]	1.8
Bunches per pulse	312
Pulse repetition rate [Hz]	50
Beam radius (r.m.s.) [mm]	2.5
Bunch length (r.m.s.) [ps]	1
Beam power [kW]	140

The positron production process starts with an electron gun and continues with the 5 GeV electron driver linac. When electron beam which comes out from this linac impinges on thin tungsten crystal, it generates a photon beam. After that, only this photon beam impinges on the amorphous tungsten target and these photons in the beam produce positrons in an electromagnetic shower. Consequently, downstream of the amorphous target, there is a capture section for the positrons created which uses an Adiabatic Matching Device (AMD). For the 5 GeV electron driver linac in positron production chain, a specific electron beam is needed. One can see the parameters desired for this beam from CLIC-CDR to produce and capture enough positrons from Table 3.1.

The parameters for the electron beam from Table 3.1 are also the parameters required for reaching the Peak Energy Deposition Density (PEDD) and determined after a systematic study of positron production as a function of amorphous target thickness the distance between crystal and amorphous targets, for different incident electron beam energies (Dadoun et al., 2009).

3.3 The Tracking Code PLACET

PLACET is a code which is written in C and a bunch of commands of C++ for simulating the dynamics of a beam in accelerating or decelerating part of a linac while the existence of wakefields, misalignments and other instabilities. It allows not only to search single and multibunch effects, but also to simulate exclusive transfer structures specific to CLIC. Also, with a number of correction schemes to investigate what emittance evolution through the beamline must be expected for given prealignments errors (Schulte, 2016).

3.4 Simple Design of the 5 GeV Electron Linac for CLIC Positron Source

Creating a FODO cell for a linear accelerator design concept by using thin lens approximation method needs multiple calculations about matrices. Also, to obtain maximum beam acceptance for a cell, phase advance per cell (μ) must be selected as 90°. One can calculate the focal length of a quadrupole magnet from $\left|\sin\frac{\mu}{2}\right| = \frac{L_{cell}}{4f}$ with a phase advance of 90° per cell and known length (L) of the FODO cell. From that calculation, by using $\frac{1}{f} = K_Q \,.\, L_Q$, strength of the quadrupole magnet can be determined.

For the first design concept of this linear accelerator of the positron source in the CLIC main beam injector complex, it was decided to use 30 MV/m cavity structures and FODO cells as mentioned in the introduction section. The first aim of this study was designing the first ever FODO cell lattice with one section for the electron driver linac without any optimization. Also, beam parameters which were mentioned in the Table 3.1, also not considered at first place, just the simulation of a single lattice section for 5 GeV linear accelerator was done.

In further steps, two focusing quadrupoles and one defocusing quadrupole were set for this initial FODO cell design and the β parameter (betatron fuction) also calculated according to the thin lens approximation as follows

$$\beta^{\pm} = \frac{L\left(1 \pm \sin\frac{\mu}{2}\right)}{\sin\mu} \tag{3.1}$$

$$\beta_x = \frac{4.4\ m\left(1 + \sin\frac{90}{2}\right)}{\sin 90} = 7.3511\ m \tag{3.2}$$

$$\beta_y = \frac{4.4\ m\left(1 - \sin\frac{90}{2}\right)}{\sin 90} = 1.4016\ m\ . \tag{3.3}$$

For calculating betatron function (β) in the equations above, phase advance (μ) for this FODO cell considered as 90° because of providing periodicity and biggest beam acceptance for the FODO lattice by considering length of cell from half of the focusing quadrupole to half of the defocusing quadrupole. Also, total length is 4.4 m for single cell including accelerating structures (cavities) and drifts. Each accelerating structure for these cells are considered about 1.5 m long and quadrupole magnets are about 0.2 m long in the considered beamline.

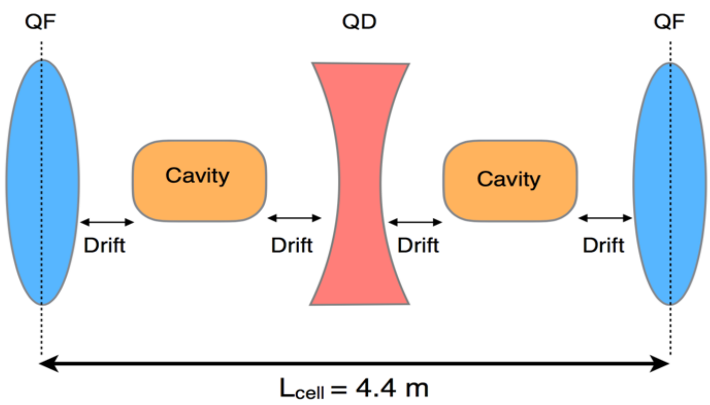

Figure 3.2. Single FODO cell example for the first inital lattice design.

By using this cell in Figure 3.2, a whole beamline was designed only containing FODO cells with one accelerating structure between two quadrupoles as demonstrated above. So, as expected, for accelerating electrons from 50 MeV to 5 GeV a very high number of quadrupoles ±160 needed because of the necessity of strong focusing for low-length cells. Moreover, this is the first ever design and it is only for testing the designed FODO cell structures in optimizing studies when energy scale increased linearly or square root of betatron function as designs evolved in the further works. Also, 1.5 m accelerating RF structures which have been considered and designed before for whole beam injector complex of CLIC were used for designing these FODO cells. There must be some space between each structure on the beamline which named as "drifts" and in this FODO cell design concept. The drifts were selected as 0.25 m as a constant value for each cell. Hence, the simple FODO cell with one accelerating structure between two quadrupole magnets becomes 4.4 m in length (accelerating structures = 1.5 m x 2 = 3.0 m drifts = 0.25 m x 4 = 1.0 m, defocusing quadrupole magnet = 0.2 m, half of focusing quadrupole magnets = 0.1 m x 2 = 0.2 m; Total = 4.4 m).

In further steps, additional longer FODO cell structures were added to the beamline consisting of three FODO cell sections at first place. When each FODO cell gets longer, strong focusing can not be provided anymore easily and weak focusing occurs between two quadrupole magnets in the FODO. With optimization calculations and simulations, less number of quadrupole magnets could be used.

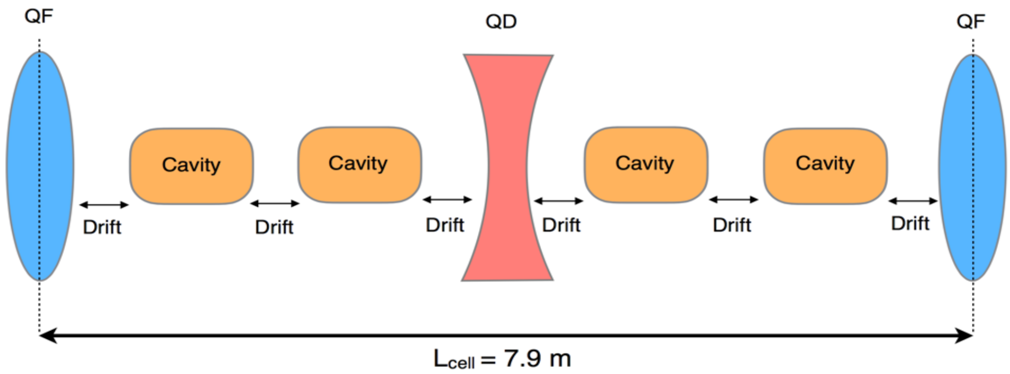

Figure 3.3. FODO cell design with two accelerating structures between quadrupole magnets which be present at the second section of design concept.

In the initial section, seven cells with one accelerating structure were used. Also, as shown in Figure 3.3, a longer FODO cell version with two accelerating structures between quadrupole magnets which is 7.9 m long and by using nine of these cells, the second section of the design concept was set.

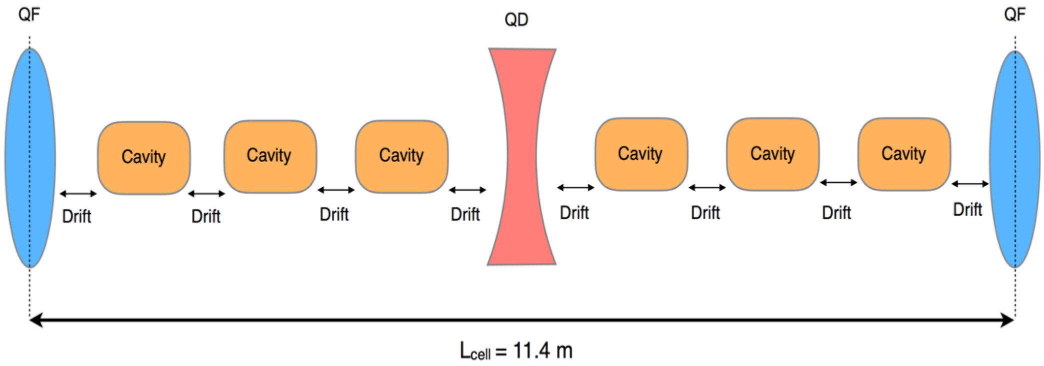

Figure 3.4. FODO cell design with three accelerating structures between quadrupoles which presents in the second section of design concept.

In Figure 3.4, third section of the design concept can be seen which consists of three accelerating structures between two quadrupole magnets and its length is about 11.4 m. For setting the third section of this design concept, ten of them were used. Moreover, first section is 30.8 m (7 cells x 4.4 m) long and took accelerating energy from 50 MeV to 0.68 GeV, second section is 71.1 m (9 cells x 7.9 m) long and increase energy from 0.68 GeV to 2.30 GeV, third section is 114 m (10 cells x 11.4 m) long and increase energy from 2.30 GeV to 5.00 GeV final value. In sketches shown in Figures 3.2, 3.3 and 3.4, the drift values were set to 0.25 m between each element in the beamline for whole design as mentioned before. The whole beamline is about 242.5 m long and 61 quadrupole magnets is used.

In further steps, for creating a whole beamline, these three defined sections must follow one another with a linear increase for the energy level from 50 MeV to 5 GeV final required energy value. The main aim was increasing the energy nearly linear and do not exceed the quadrupole magnet field of maximum of 1.2 T when designing these three different FODO cell sections. In first and second sections of the machine, quadrupole magnet field strength optimized for 0.5 T, but in the last quadrupole of third section, it reaches about value of 1.03 T which is not exceeds the maximum value of 1.2 T. Simple calculation for accepted quadrupole strength according to energy level that one FODO cell can be reach the maximum desired quadrupole field value. Beam pipe diameter was taken as 2 cm optimal value for an electron beam which is lower than 0.4 cm maximum of beam radius value along the beamline for this initial design. Parameters such as quadrupole magnet field for proper quadrupole magnet focusing strength values were calculated as follows

$$\left|\sin\frac{\mu}{2}\right| = \frac{L_{cell}}{4f}$$

$$\Rightarrow\ L_{cell} = 4.4m,\quad \mu = 90° \tag{3.4}$$

$$\left|\frac{\sqrt{2}}{2}\right| = \frac{4.4\ m}{4f}$$

$$\Rightarrow\ \frac{1}{f} = 0.6428\ m^{-1} \tag{3.5}$$

$$\frac{1}{f} = K_Q\,.\,L_Q$$

$$\Rightarrow\ 0.6428\ m^{-1} = K_Q\,.\,0.2\ m \tag{3.6}$$

$$K_Q = 3.2141\ m^{-2}$$

$$K_Q[m^{-2}] = 0.2998\ \frac{B\ [T]\ /\ r_Q[m]}{E_{out}^{i}[GeV]}\ . \tag{3.7}$$

From the Equation (3.7), if the magnetic field is wanted to be lower than 0.5 T for example, the output energy can be calculated from known quadrupole strength K_Q and selected quadrupole radius value r_Q;

$$E_{out}[GeV] = 0.2998\ \frac{0.5\ T\ /\ 0.05\ m}{3.2141\ m^{-2}}$$

$$= 0.93\ GeV \tag{3.8}$$

As seen from calculation in the Equation (3.8), quadrupole field strength must be lower than 0.93 GeV if the first section of the design wanted to be not outperform the value of 0.5 T. Hence, in first section of this initial design, the energy value was reached 0.68 GeV as maximum at the end of the first section which was much lower than the desired value. Moreover, the quadrupole radius value r_Q was selected as 5 cm

(10 cm in diameter) for this linac and it was considered as an optimal value for maximum beam radius and calculated as follows

$$r_Q[m] = 0.2998 \frac{0.36}{K_Q[m^{-2}]\, E^{i}_{out}[GeV]}. \qquad (3.9)$$

3.4.1 The Matching Method and Matching Section Between Two Different Sections of Linac

Different β (betatron fuction) values which are varied for each FODO cell section because of the different length of FODO cell designs, there must be a matching sector between each FODO cell section from end of the last one in the current part to the starting point of other one in the new part.

The idea is trying to match different β values of different linac sections with varied FODO cells to each other with a free-part consisting from quadrupole magnets and drifts which is shown in Figure 3.5. For providing optics which leads β_x and β_y values remain periodically, previous section's last half quadrupole magnet was added to the matching code in simulations with PLACET program and it was tried to match it to the new section which also starting with a half-quadrupole as well as different β_x and β_y values.

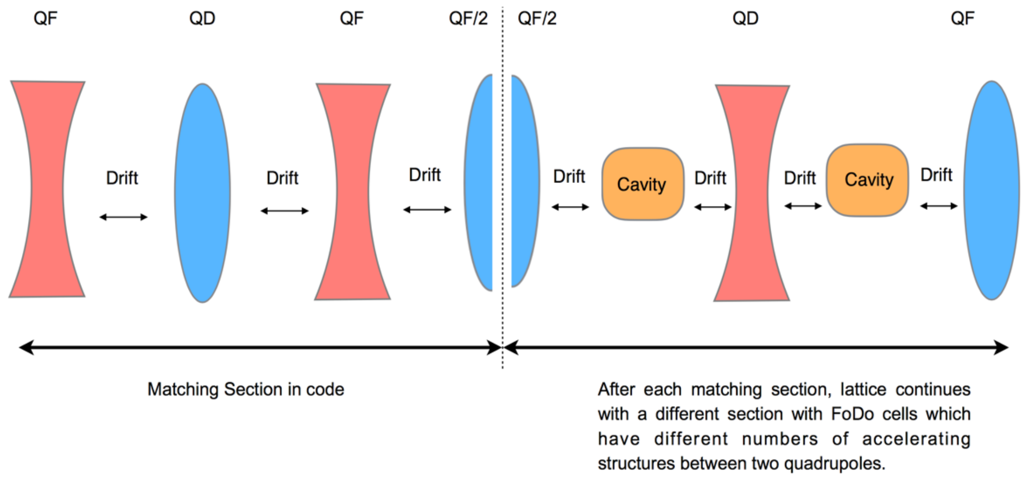

Figure 3.5. The matching section for different parts of linac.

To match β_x and β_y for two different FODO lattice parts, PLACET reads the "beam.out" data file which includes only the parameters of previous FODO section and matches betatron values to the new calculated ones that were desired for the new part. This method perfectly matches different sections to each other by using and finding perfect values for the constraints that were determined in the code such as strength of the quadrupole magnets and length of the drifts. Consequently, when matching done with simulations, betatron function had to be move along periodically through whole beamline and selected initial values for ε_x (emittance along x-axis) and ε_y (emittance along y-axis) values had to be stable. If there is significant increase for these values along the beamline, that indicates an instability for the beam.

3.4.2 Periodic Betatron Function and Emittance Evolution

The periodic betatron function for the beamline can be seen in the left side of the Figure 3.6 and after each matching section. The beamline moves along with a new periodic betatron function value because of FODO cell sections which comprise longer-cells. In matching parts, a little leap for betatron function results in because of the imperfections when simulating matching sections with the code, but that leap is not big enough for losing or distort the electron beam because beam radius is at a very lower value than (about 4000 µm = 0.4 cm) beam pipe which considered as 2 cm.

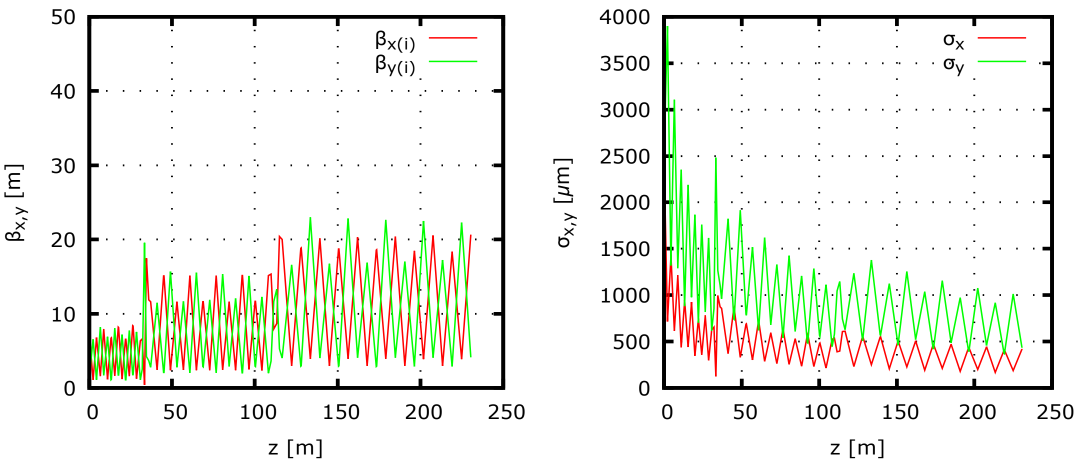

Figure 3.6. Betatron function value through beamline (left), beam size evolution through beamline (right).

Emittance is the area or the volume in the phase space ellipse of the particle beam which characterizes beam's size. It is also used to describe a beam because the emittance is invariant if there is no dispersive or cooling forces exist (U.S. Particle Accelerator School (USPAS), 2012). Moreover, evolution of emittance values through the beamline is one of the most important things that distorts the beam. This value had to be stable along the beamline, any increasement of emittance above 10% through the machine can not be acceptable.

It is also important to keep emittance stable through the beamline for a linear accelerator while adding different FODO cell sections end to end. If emittance grows too much throughout the beamline, this causes beam size to increase and which is a bad issue for the beam. It can even lead beam loss in the walls if beam size increases much higher than the width of the beam pipe that considered for the design.

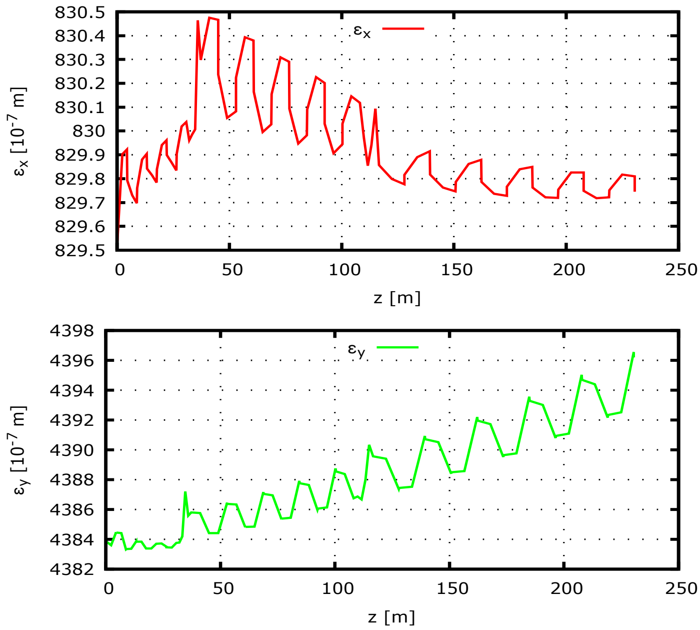

Figure 3.7. Emittance evolution through the beamline.

As shown in Figure 3.7, ε_x was taken as 829×10^{-7} m·rad and ε_y was taken as 4384×10^{-7} m·rad according to suggestions given in the CLIC beam physics group meeting. Graphic is sketched for the emittance evolution through the beamline in both x-axis and y-axis from output data of the PLACET simulation program. For initial design of the linac only with three FODO cell sections shows nearly stable beam emittance values both x-axis and y-axis through the beamline. This indicates matching sections between different part of the linac design were matched together precisely by using PLACET.

3.4.3 Impact of Misalignments on the Beamline for the Simple Design

In this design task for linear accelerator, it is important to work on the misalignments of beamline elements. The aim of this study is really important for determining error tolerances of designed beamline when some element in it set up with an initial or random error. Consequently, components that were created the beamline such as quadrupole magnets, cavities, beam positioning monitors (BPM) might be set up with an error. In simulations, effects of these set up errors and instabilities is had to be examined.

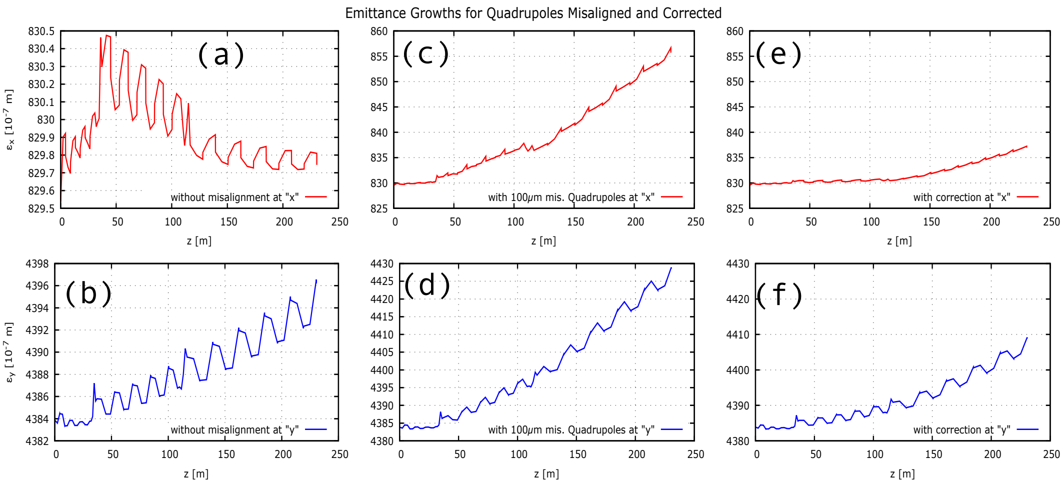

Figure 3.8. Emittance evolutions when each quadrupole in the beamline 100 μm randomly misaligned and corrected a) and b) without beam offset or misalignment, b) and c) with 100μm random quadrupole misalignments, e) and f) after correction with dipoles.

Furthermore, for determining error tolerances, focusing and defocusing quadrupoles in the beamline were misaligned 100 μm randomly. Effects of misalignments and corrections are shown in Figure 3.8. In graphs (a) and (b), emittance values of beamline were shown without misalignments. In graphs (c) and (d), each quadrupole was misaligned 100 μm randomly. There was a little increase in the emittance value which is ~3%. About 10% of emittance growth in the beamline is acceptable while doing simulations. From graphs (e) and (f), beamline errors were corrected by adding dipole corrector magnets after each quadrupole in the beamline, and for observing the correction, the beam position monitors with 100 μm resolution were added.

The beam might be focused or defocused to an undesired point because of the given random set up errors for each quadrupole magnet. The dipole corrector magnets are kicking the wrong-focused beam to the correct path. As a result, emittance values both x-axis and y-axis were corrected to initial given values. BPMs is shown that the correcting with dipoles with one-to-one correction technique was worked. One-to-one correction is a technique that means for each quadrupole in the beamline, there is a dipole corrector magnet for correcting possible set up errors.

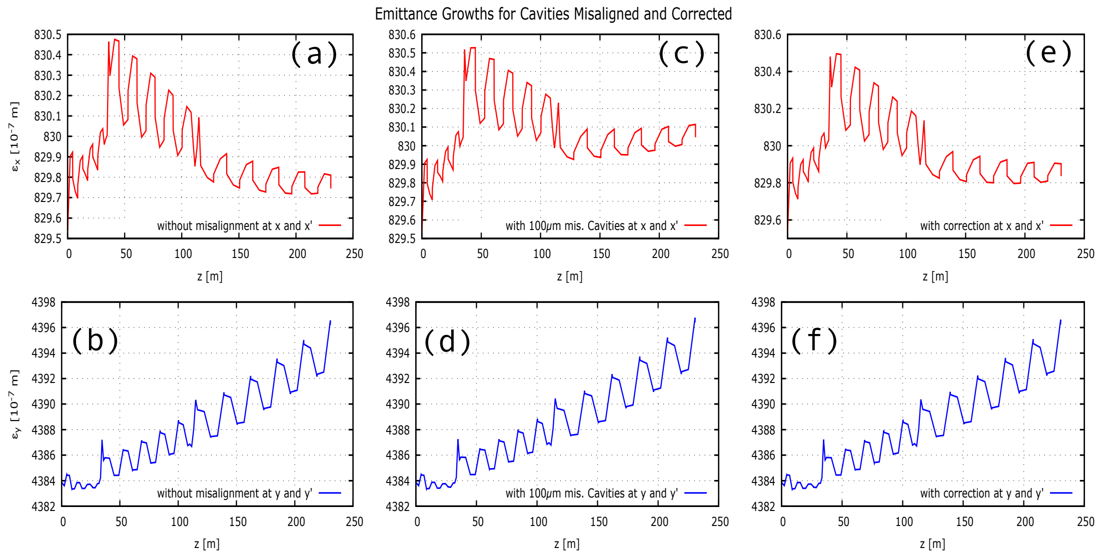

Figure 3.9. Emittance evolutions when each cavity in the beamline 100 μm randomly misaligned and corrected a) and b) without beam offset or misalignment, b) and c) with 100μm random cavity misalignments, e) and f) after correction with dipoles.

In simulations, each cavity also misaligned for about 100 μm randomly and results in graphics is shown in Figure 3.9. Graphs (a) and (b) are showing the default beamline emittance values. According to graphs (c) and (d), misaligned cavities have not effect at all on the beamline for increasing emittance. As seen in graphs (e) and (f), corrector dipole magnets corrected this low emittance growth to the default level.

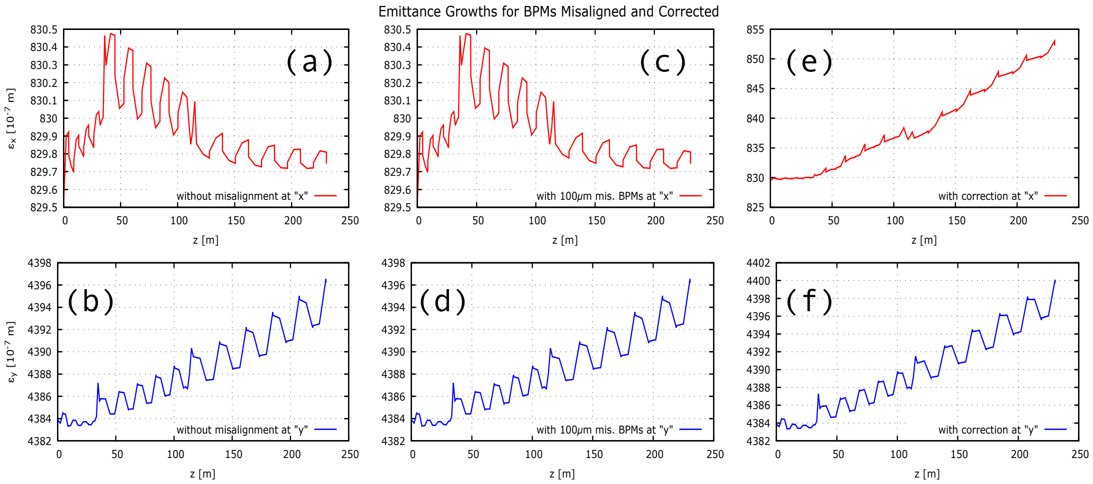

Figure 3.10. Emittance evolutions when each BPM in the beamline 100 µm randomly misaligned and corrected a) and b) without beam offset or misalignment, b) and c) with 100µm random BPM misalignments, e) and f) after correction with dipoles.

In Figure 3.10, graphs (a) and (b) stands for default beamline emittance values. BPMs has no effect when they were misaligned shown in graphs (c) and (d), but at graphics (e) and (f), a small increase in emittance can be seen. Hence, that increase from BPMs when beam corrected with corrector dipoles, they were acted like focusing quadrupoles and they are seen the beam from a different position in the way that the beam was kicked.

BPMs are locating a beam of charged particles in the beam pipe, so they were here for only locate and monitorize the position of the beam. Besides, when dipole correctors gave no kick because there are no misalignments for any quadrupole magnets in simulations to correct the wrong-focused beam in the beamline. Also, all simulations for beamline were considered and done for 100 machines which means simulations were done 100 times and beam was transferred randomly through the beamline about 100 times. As a result, BPMs have no harmful effect on emittance growth in these simulations result.

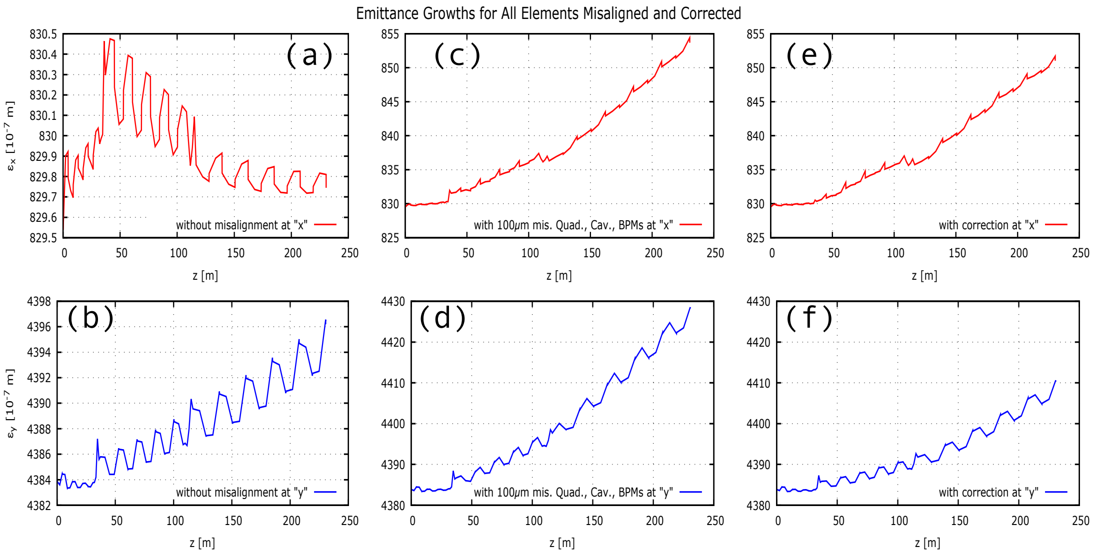

Figure 3.11. Emittance evolutions when all components together (quadrupoles, cavities and BPMs) in the beamline 100 µm randomly misaligned and corrected a) and b) without beam offset or misalignment, b) and c) with 100µm random quadrupoles, BPMs and cavities misaligned together, e) and f) after correction with dipoles.

In Figure 3.11, graphs (a) and (b) are shown the default beamline emittances for both x and y axes. In graphs (c) and (d), cavities have very little effect on emittance growth and also no increase from BPMs side. When all components in the beamline were misaligned together, the biggest emittance growth is coming from focusing and defocusing quadrupoles. In this scenario, the beamline was affected slightly more compared to when quadrupoles randomly misaligned about 100 µm. From graphs (e) and (f), one can conclude the one-to-one correction with corrector dipole magnet method was worked and emittance values came back nearly to the default level.

As a result of these misalignment studies for initial design of this linac, the strong focusing of the quadrupole magnets does not let the emittance to increase more than ~3%. In addition, when wakefield effect calculation added to simulation code for 2 GHz S-band accelerating structures, it does not distort the beamline above acceptable 10% emittance growth level because of the strong focusing and the precise matching simulation between FODO cell sections. Also, when wakefields were included, the beam will be transferred from the starting point to the end of the linac without a big emittance growth even if there are set up errors for components in beamline about 100 µm tested value which is optimal error for the set up misalignments.

3.5 Optimizing Parameters and Performance of the 5 GeV Electron Linac and Beam Dynamics Studies

In this part of the studies, the main goal is to develop the initial design with distinctive layout options. It is also important that reducing any number of beamline components such as quadrupole magnets in the beamline decrease the total cost of the linac.

Parameters from the first design concept is not changed too much except the emittance values for both x and y axes. They both taken as 1000×10^{-7} m·rad which are optimal values for an electron beam that considered to come from an electron gun. However, this electron gun considered before for 5 GeV electron linac have not been studied yet. Hence, taking nominal values for emittances from the electron gun are important because those values determine the beam size value for the design. Bigger emittance values may surpass the beam pipe size which can cause instability problems and beam loss.

Two different partitioned designs were considered, one with 5 different FODO cell sections and the other one with 4 different FODO cell sections. Moreover, for both different designs, the accelerating gradient value was selected as 20 MV/m because 30 MV/m gradient value might be hard to reach with normal conducting accelerating structures and it will cost more power to accelerate. This will also increase operation costs because more klystrons will be used for generating more power. Consequently, 20 MV/m accelerating gradient value was selected for optimization study. However, with 20 MV/m accelerating gradient, one accelerating structure about 1.5 m in length, can accelerate the beam less than 30 MV/m gradient value accelerating structures which result to increase the total length of the linac.

In the first design option which consists of 5 different FODO cell sections and they contain 2 FODO cells with 2 accelerating structures, 2 FODO cell with 6 accelerating structures, 2 FODO cells with 12 accelerating structures, 3 FODO cells with 18 accelerating structures and 3 FODO cells with 24 accelerating structures, consecutively. At first part, one cell is about 4.4 m long and at the last part one cell is about 42.9 m long. β function parameter is also enhanced by a function as follows

$$\beta_f = \beta_0 \sqrt{\frac{E_f}{E_i}} \tag{3.10}$$

which indicates the β increased by factor ten by using the Equation 3.10 above and shown below according to the final and initial energies from starting of the structures to the end part of the structures of the linac.

$$\beta_f = \beta_0 \sqrt{\frac{5.00\ GeV}{0.05\ GeV}} \quad \Rightarrow \quad \beta_f = \beta_0 \cdot 10 \tag{3.11}$$

With this enhancement of betatron function value according to the Equation (3.11), final value was set 10 times higher than initial value by using square-root of final energy over initial energy of the linac. Moreover, for reaching these achievement, one FODO cell must be very long at last one or two parts of the designs which means higher β value coming from these parts. These increase of the β will cause stress on the beam at the last parts of the machine and if casual setup errors ~100 μm was initially given to the simulations, the emittance will grow even more. But these errors could be fixed with adding corrector dipole magnets after each quadrupole in the beamline.

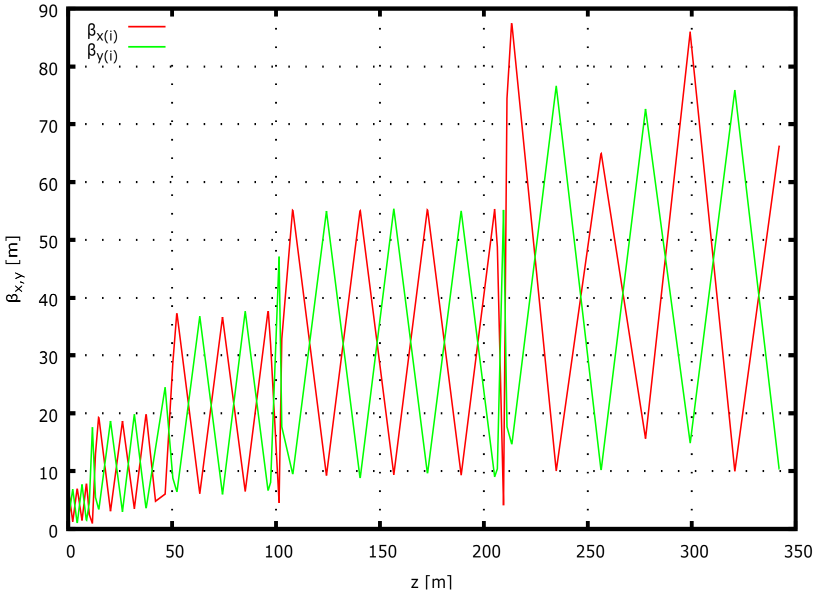

Figure 3.12. Betatron function evolution through the beamline for the design with 5 different FODO cell sections.

Figure 3.12 shows the periodic betatron functions in different FODO lattice sections. There is no deformation at all except the matching areas which connects two different FODO lattice sections with different betatron values. In addition, there is no initial errors or setup errors in this situation. At last part of the design with 5 FODO cell sections leads to a little fluctuation which can be seen in the Figure 3.12. This fluctuation of betatron function is coming from the little emittance growth in last section. Also, using of longer FODO cells about 44.4 m each in the last section have an effect for this fluctuation of betatron function.

Emittance evolution for the design with 5 different FODO cell sections can be seen in Figure 3.13;

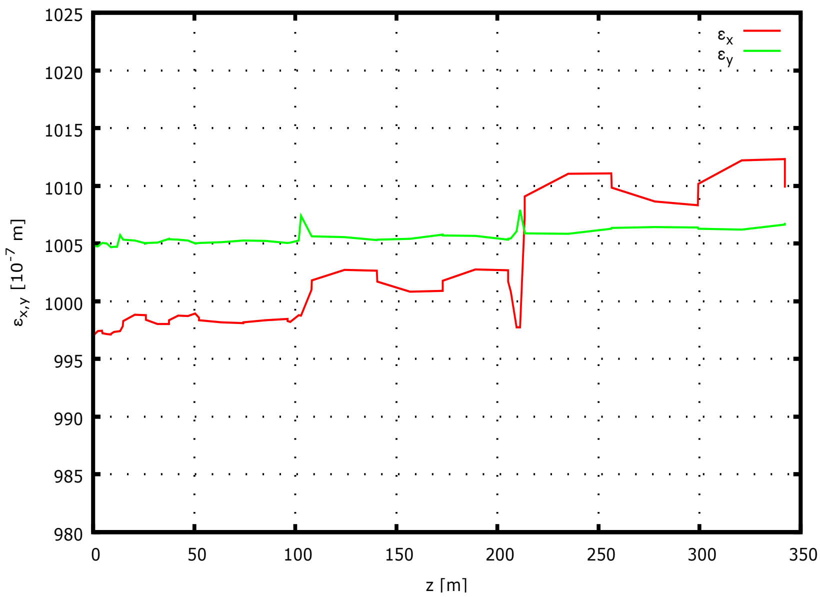

Figure 3.13. Emittance evolution through the beamline for the design with 5 different FODO cell sections.

From Figure 3.13, little emittance growth can be seen after the 4th FODO cell section which starting to increase after 200th meter of the machine. Here, starting emittance values for both ε_x and ε_y are 1000x10^{-7} m·rad in both planes and the resulting emittance values for both x and y is maximum 1010x10^{-7} m·rad at the end of the machine. This indicates 0.01% emittance growth which is a very little growth while 10% growth is can be acceptable in these situations.

According to this beam emittance values, beam size $(\sigma_{x,y})$ values through the beamline of the machine are shown in Figure 3.14 . If there is a fluctuation in emittance values through the beamline, the beam sizes will also fluctuate. However, in this design without beamline errors, we have suitable beam size values through the whole beamline which are reached maximum value about 2500 μm (2.5 mm) while our beam pipe dimater was considered as 2 cm.

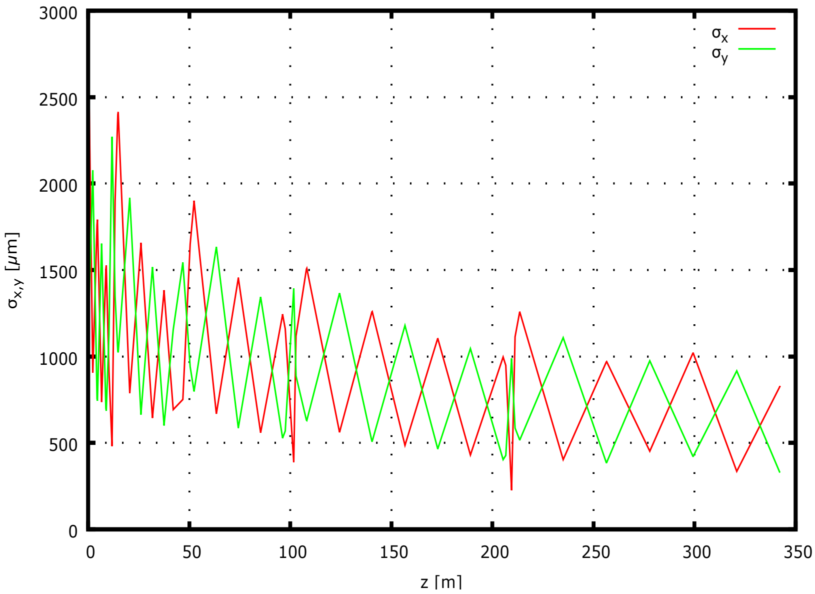

Figure 3.14. Beam size evolution through the beamline for the design with 5 different FODO cell sections.

Consequently, with this whole beamline design with 5 different FODO cell sections, our goal was to enhance the betatron function by factor 10. From starting of the machine to the end, this goal is achieved. Because of very long FODO cells used at 5th section of the design, emittance is growth a little bit and this will also increase the emittance when setup errors are involved in simulations for testing the effects of beam instabilities.

As an alternative design to the previous one, a beamline for this machine with 4 different FODO cell sections is also considered. This design will not increase the betatron function value by factor 10, but it will be increased nearly factor 10 while using slightly longer FODO cells at the end part of this design than the end part of the previous design. So, matching betatron functions become easier and the periodicity of it was kept because of the slightly longer cells that used at the end part of this alternative design.

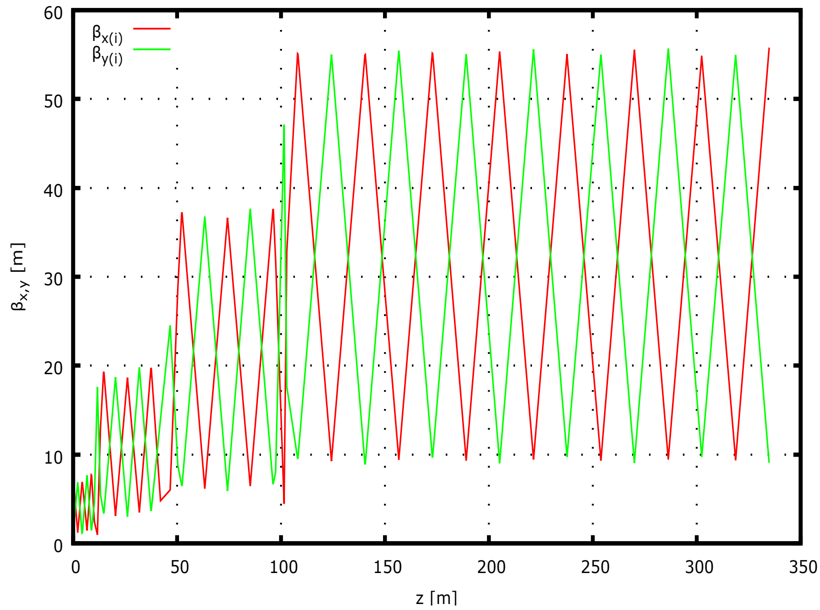

Figure 3.15. Betatron function evolution through the beamline for the design with 4 different FODO cell sections.

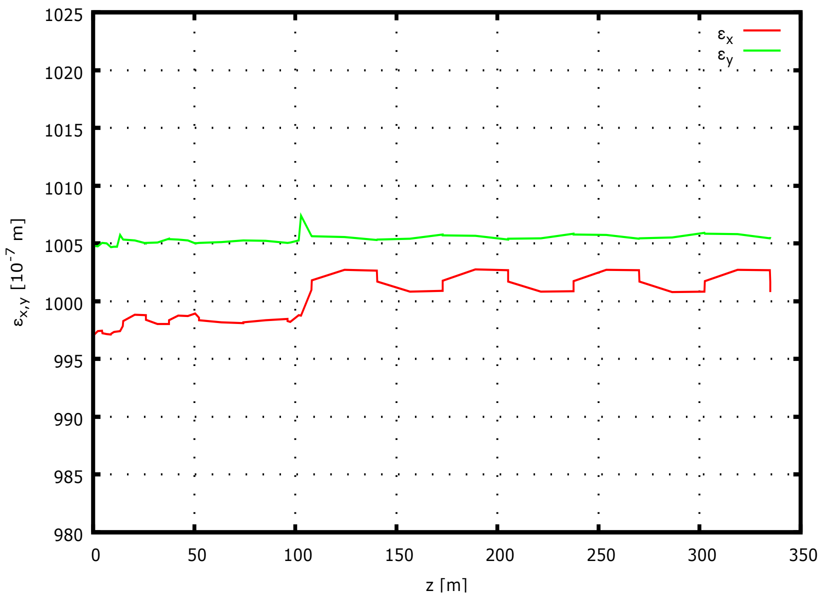

Figure 3.16. Emittance evolution through the beamline for the design with 4 different FODO cell sections.

The goal of this alternative design is to provide more stable betatron function and beam sizes since slightly shorter cells than the previous one were used. From Figure 3.15, the betatron function evolution shown with a graph and it is more stable and perfectly periodic, but number of quadrupole magnets is less than the 5 section FODO cell version. Also, from Figure 3.16, the emittance can be seen as much more stable. The beam size shown in Figure 3.17 is also more stable than the previous design's resulting values, too.

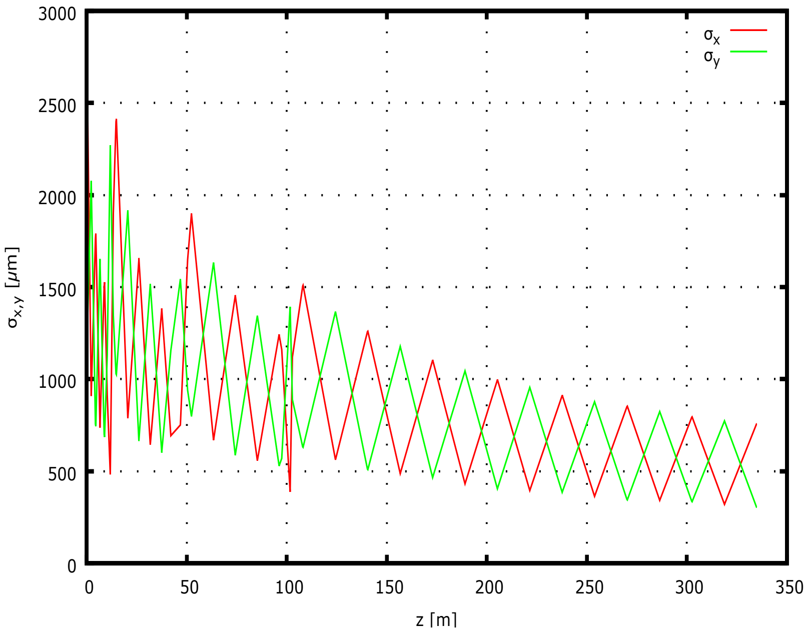

Figure 3.17. Beam size evolution through the beamline for the design with 4 different FODO cell sections.

Table 3.2. Basic specifications of three different designs for 5 GeV electron linac.

	5 GeV design with three FODO sections	5 GeV design with five FODO sections	5 GeV design alternative with four FODO sections
Accelerating Gradient	30 MV/m	20 MV/m	20 MV/m
# of Quadrupoles	61	45	43
Total Length	242.5 m	342 m	334 m
Filling Factor	71.5 %	72.4 %	74.5 %

If we look from another perspective, in cost terms, if number of quadrupole magnets are increased in the beamline that means the beamline will cost more price when setup is done. So, according to some of their basic parameters, comparison of these three different designs given in the Table 3.2.

From the Table 3.2, selected accelerating gradient which provided from normal conducting accelerating structures and number of used quadrupole magnets for whole beamline for different design options can be seen. Total length of the linear accelerator designs including matching sections between different FODO cell parts and also filling factor which is the ratio of accelerating structures over whole beamline. Thus, when we compare 4 section one to the 5 section one, quadrupole numbers, the length of the linac and filling factor value are very close to each other

3.5.1 Matching the Beam Size for Target

By adding a different matching section to the end of the linac, the desired beam size for the tungsten target after this part was given in Table 3.1 as a round beam with 2.5 mm radius. To provide this beam size for impinging electrons to the tungsten target and producing positrons, different betatron values of desired 2.5 mm radius beam size and our beam's size at the end of the designed linac must be matched with simulations.

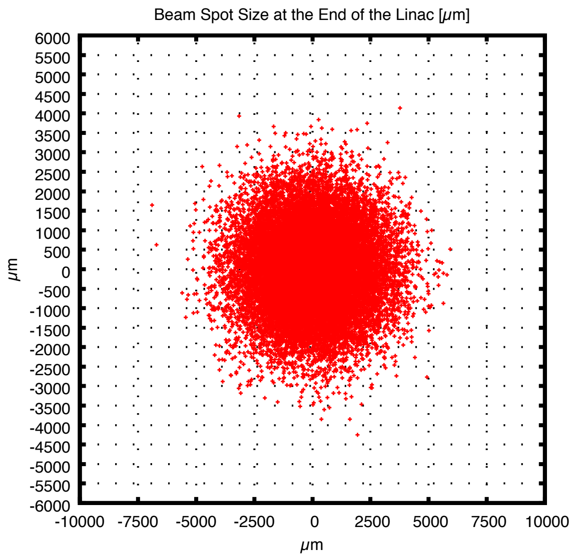

Figure 3.18. Beam spot size for tungsten target at the end of the linac about 2500 μm (2.5 mm) radius.

In Figure 3.18, the resulting beam spot size as 2.5 mm radius can be seen and this data for the graph is taken from the end of the linac. This spot size is for reaching best positron yield when electrons in the beam impinging on the tungsten target.

3.5.2 Impact of Misalignments on the Beamline for the Optimized Designs

Instabilities in beamlines have bad effects on beam. The most important part and main goal of the study is testing wakefield effects on designed layout of beamlines. When wakefields are in presence in simulations, longer FODO cells with larger betatron functions affected more because of the low focusing due to longer distances between quadrupole magnets. Also, beam size may growth very large which may cause beam loss on the walls, non-periodic betatron functions and low quality beams. In this part of the studies, designed beamlines tested with initial beam errors as well as setup errors and results will be discussed.

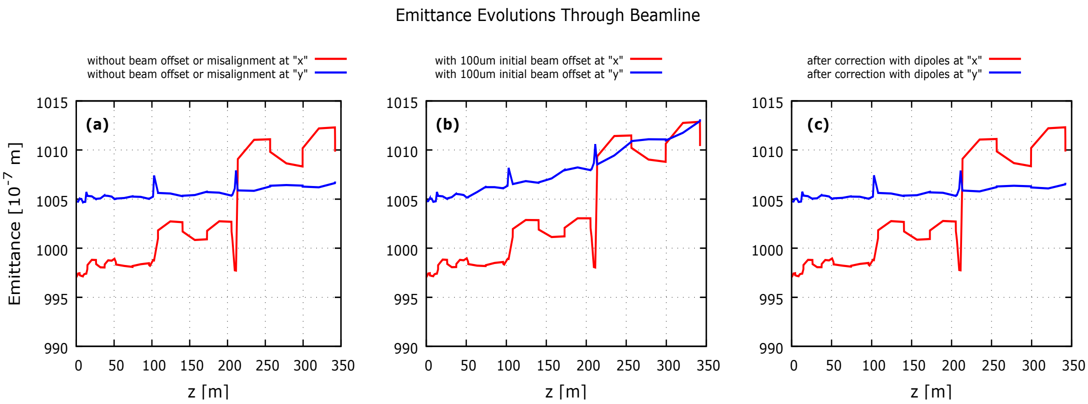

Figure 3.19. Emittance evolutions through beamline for design with 5 FODO cell sections when 100µm initial beam offset and correction of errors with dipole magnets a) without beam offset or misalignment, b) with 100µm initial beam offset, c) after correction with dipoles.

In Figure 3.19 above, graph (a) shows that the default beamline and there is no error for the beam, but at x-axis small emittance growth was seen because of the longer cells at the last part of FODO cells about ~45 m each and because of the non-perfect betatron function. In graph (b), 100 µm initial beam offset was given to the beam at the beginning of the machine. More, wakefield effect calculations are included in the code when simulations were done. Thus, emittance values increased a little bit and it is an acceptable growth, no beam deflections at all. Also, from graph (c), one-to-one correction with dipole magnets and effects of correction can be seen on the emittance values which were recovered to the initial values for both x-axis and y-axis.

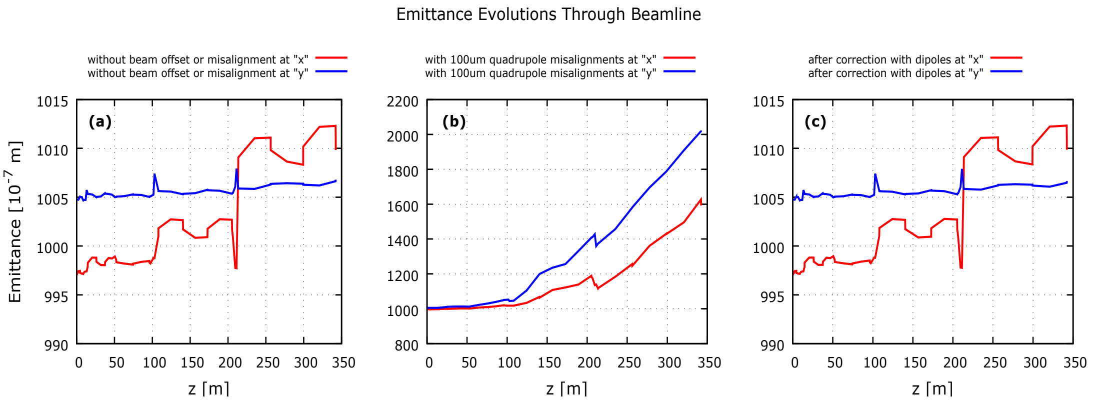

Figure 3.20. Emittance evolutions through beamline for design with 5 FODO cell sections when all quadrupole magnets 100µm randomly misaligned and correction of errors with dipole magnets a) without beam offset or misalignment, b) with 100µm quadrupole misalignments, c) after correction with dipoles.

Default emittance values without any misalignment errors can be seen in Figure 3.20 from graph (a). However, when all quadrupoles in the beamline 100 µm randomly misaligned together in the simulations, the effects are very harmful to the beamline. Emittance is grown nearly 100% and that means this kind of designs with longer FODO cells and with weak quadrupole focusing are not stable when wakefield effects are in presence in simulations. In addition, when one-to-one correction method which means one dipole magnet after each quadrupole magnet in the beamline was implemented to the code. The effect of correction from dipole magnets that were added to the beamline can be seen in graph (c) in Figure 3.20. Hence, the applied correction method with dipole magnets are very powerful here and correct beam emittance values nearly 100% to default values.

There is another error check for the beamline were also done for the case when all components of beamline which are BPMs, cavities and quadrupole magnets misaligned together randomly. The effects of all components misaligned together is shown in Figure 3.21;

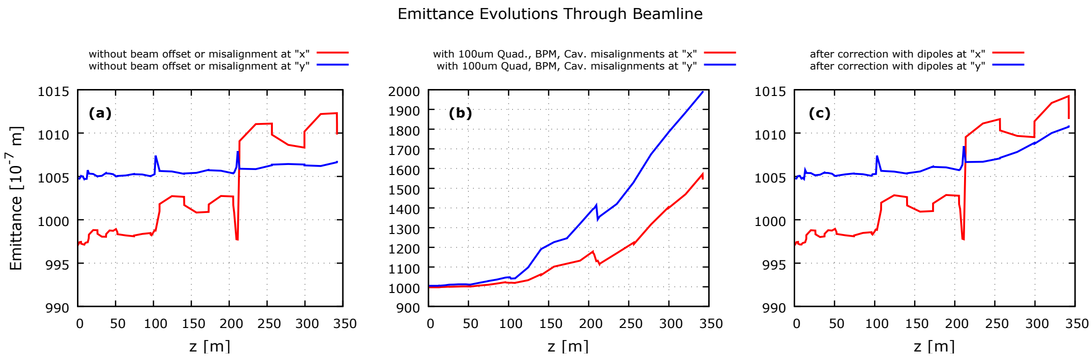

Figure 3.21. Emittance evolutions through beamline for design with 5 FODO cell sections when all components (BPMs, quadrupoles and cavities) 100µm randomly misaligned and correction of errors with dipole magnets a) without beam offset or misalignment, b) with 100µm quadrupole, BPM and cavity misalignments, c) after correction with dipoles.

In Figure 3.21, graph (a) shows the default emittance values without any errors for design with 5 FODO cell sections. Big effects of wakefields can be seen in graph (b) and emittance values were increased nearly 100% when all components randomly misaligned together at the same time about 100 µm. However, when one-to-one correction method is applied into simulations, dipole magnets corrects the beam and emittance values nearly become same as default values with a little error which is lower than 0.1% and it is an acceptable emittance growth.

In other part of this study, design with 4 FODO cell sections is also tested for how errors and misalignments in the beamline components will effect the beam and emittance.

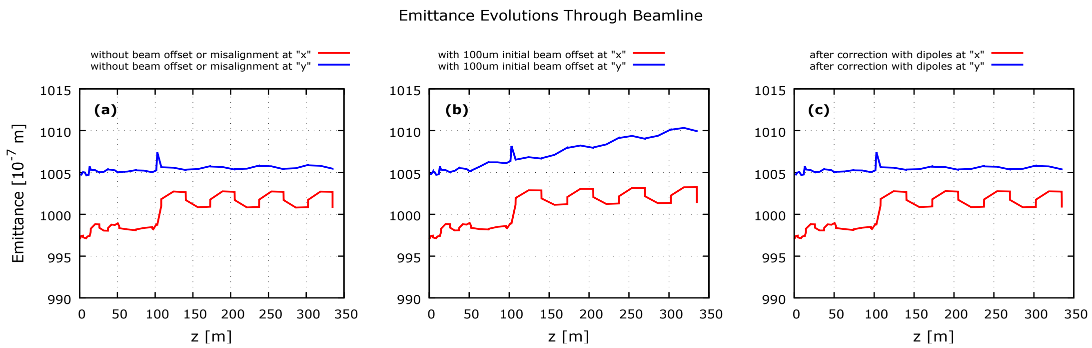

Figure 3.22. Emittance evolutions through beamline for design with 4 FODO cell sections when 100µm initial beam offset and correction of errors with dipole magnets a) without beam offset or misalignment, b) with 100µm initial beam offset, c) after correction with dipoles.

When initial beam offset is given to the beam, correction of errors with dipole magnets and resulting emittance values are shown in Figure 3.22. Graph (a) shows the default beamline emittance with no errors, but in graph (b) 100 μm initial offset is given to the beam as an error and emittance values are not increased at all. When one-to-one correction method is applied to the beamline, beam emittances are restored to the default values and correction is perfectly done as shown in graph (c) in Figure 3.22.

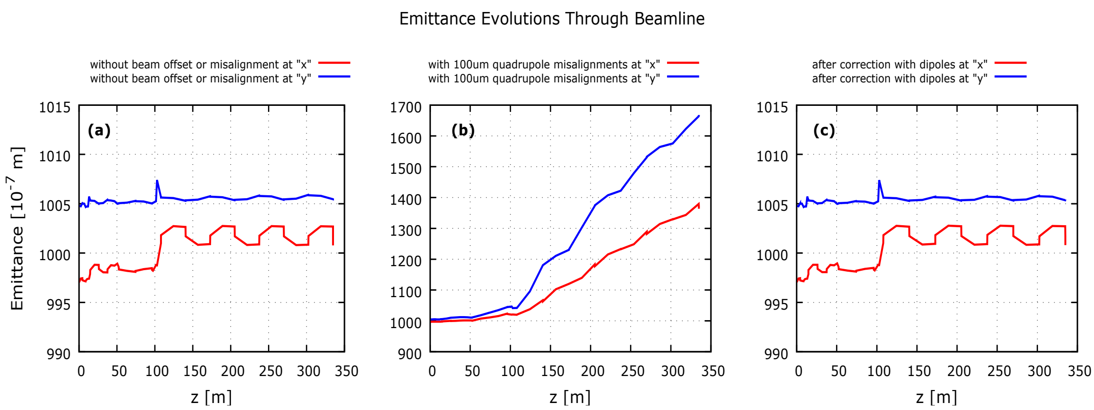

Figure 3.23. Emittance evolutions through beamline for design with 4 FODO cell sections when all quadrupole magnets 100μm randomly misaligned and correction of errors with dipole magnets a) without beam offset or misalignment, b) with 100μm quadrupole misalignments, c) after correction with dipoles.

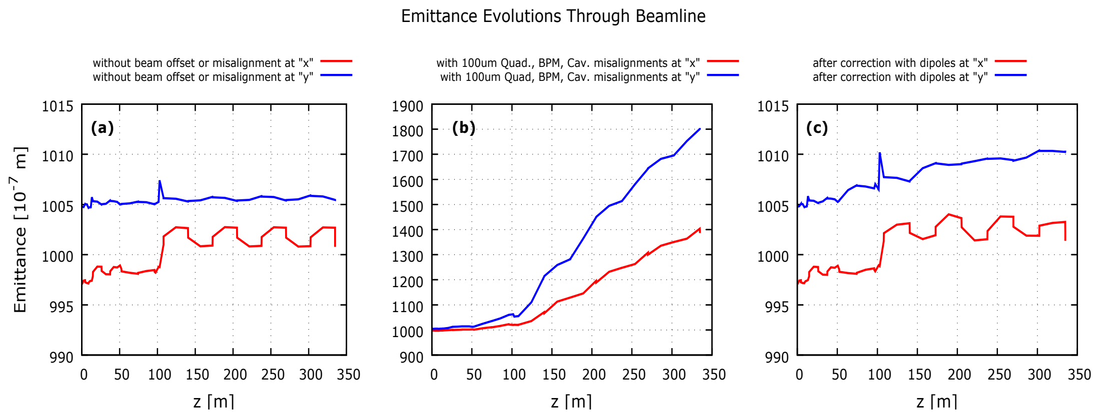

Figure 3.24. Emittance evolutions through beamline for design with 4 FODO cell sections when all components (BPMs, quadrupoles and cavities) 100μm randomly misaligned and correction of errors with dipole magnets a) without beam offset or misalignment, b) with 100μm quadrupole, BPM and cavity misalignments, c) after correction with dipoles.

From both Figure 3.23 and Figure 3.24, default emittance values can be seen in graph (a) and in graph (b) for both figures show 100 μm random quadrupole magnet misalignments and all components 100 μm randomly misaligned at the same time, respectively. Emittance growth for both quadrupoles and all components growth emittance around 90-95% which is very higher value, but lower than 5 FODO cell section design. In graph (c) for Figure 3.23, only quadrupoles were misaligned and one-to-one correction was worked perfectly. However, for graph (c) in Figure 3.24, after the correction with dipole magnets, a little excessing value for emittance can be seen if compared to the default emittance values in graph (a). This increasement is coming from some of the cavities that were acted like focusing quadrupoles and giving some wrong directioned focus to the beam. Thus, that increase is inevitable in simulations even if one-to-one correction is applied and beam was directed to the correct position because BPMs were also seen the beam from different aspect after correction.

4. RESULTS AND DISCUSSION

In this part, results of designed beamlines for 5 GeV electron linac for CLIC positron source will be discussed from the perspective of how it was designed and optimized.

In the beginning, preliminary design of the beamline without any optimizations was done and this design was focused only for achieving mentioned parameters of this linac such as beam current, emittance, number of particles per bunch etc. After that, this preliminary design's performance and effectiveness were optimized by changing the FODO lattice sections with different and increasing lengths. During this optimization study, performance of the beam delivery between structures without any distortions and providing a perfect periodicity of betatron functions among different FODO sections were very important. In addition, while betatron functions between different FODO sections were tried to match one after other. In PLACET program, the code for matching method was a bit old and doing a different calculation for matching by using ratio. The code section in it which is convenient for matching different betatron function values was renewed during this thesis study and a contribution was also provided. After that improvement, different betatron functions can be matched with PLACET about $\sim10^{-29}$ precision which was a very well proximity when two different betatron functions were tried to match each other. Thus, after a fine matching was provided between betatron functions and beam was delivered nicely through designed structures, optimization of parameters and performance was coming to the forefront such as reducing the number of quadrupoles in beamline for decreasing total cost of the linac. Then, design was considered as a little longer in total but with reduced number of quadrupole magnets. To provide less number of quadrupole magnets, number of lattice sections with longer FODO cells were increased. While reaching 5 GeV energy value for the linac, betatron function values were tried to increased by factor 10 by the Equation 3.10. More, while trying to achieve 10 times higher betatron function from the starting of the beamline to the end, less quadrupole magnets were used because the longer FODO cells that used for increasing the betatron functions.

In addition, performance of this longer but cost-effective design version was tested with wakefield effects calculations. Increasing the betatron function value by factor 10 from the beginning to the end was stressed beam to the edge. For testing errors, some set up misalignments of beamline components were given in simulations. Thus, these set up errors were increased the emittance and distorted the periodicity of betatron functions much more when the wakefield effects were included. Besides, one-to-one correction (one dipole magnet after each quadrupole magnet) method with corrector dipole magnets was applied for correcting these errors in simulations for testing performance of the beamline. Error and misalignment studies were shown that the one-to-one correction with dipole magnets always corrected beam to the default direction and form although weak focusing from quadrupole magnets because of the longer FODO cells which sharply increased wakefield effects on the beamline. In short, these 100 μm setup errors that were tested for beamline made big impact on beamline, but did not affect too much that could not be corrected in normal conditions with corrector dipoles in beamline.

To conclude, design and optimization of 5 GeV electron linac to produce positrons for CLIC is deisgned for the first time in CLIC collaboration. This preliminary design is also optimized with different layouts and tested under effects of distortions for the beam.

5. CONCLUSIONS AND RECOMMENDATIONS

Adjusting parameters in the design layout of structures to transfer a fine beam through the designed linac is an important part in the conceptual design of an accelerator. This work is the first work done on the preliminary design for a linac which was only in terms of estimated parameters in CLIC-Conceptual Design Report. Different layout schemes of linac were considered and designed. Each of these designed beamline layouts of 5 GeV electron linac is optimized with various choice of parameters. Consequently, optimized quadrupole numbers from preliminary first design to optimized designs are reduced 30% which will also decrease the total cost of the linac. In conclusion, how errors in setup and instabilities are effecting the designed beamlines as well as the beam's quality is studied in this thesis.

6. REFERENCES

Bayar C et al. (2017) "Design and Optimisation of the Positron Production Chain for CLIC from the Target to the Damping Ring", Nuclear Instruments and Methods in Physics Research, A, ISSN:0168-9002:56-62

CERN (2012) A Multi TeV Linear Collider Based on CLIC Technology CLIC Conceptual Design Report, CERN-2012-007, Geneva

Dadoun O et al. (2009) "Study of a Hybrid Positron Source Using Channeling for CLIC", CLIC-Note-808, September 2009, Geneva

International Linear Collider (ILC), http://www.linearcollider.org/ , 1 February 2018

Rossbach J and Schmüser P (1994) " Basic Course on Accelerator Optics", Cern Accelerator School Fifth General Accelerator Physics Course, 7-18 September 1992, Finland

Schulte D (2016) The Tracking Code Placet Version 1.00, http://svn.cern.ch/guest/clicsw/trunk/placet/doc/placet.pdf, 10 February 2018

SLAC Linear Collider (SLC), www-sldnt.slac.stanford.edu/alr/slc.htm, 5 February 2018

Spentzouris L (2012) U.S. Particle Accelerator School (USPAS): Lecture - Emittance, http://uspas.fnal.gov/materials/12MSU/emitlect.pdf, 5 February

Wangler TP (1998) Principles of RF Linear Accelerators, First Edition, John Wiley and Sons Incorporation, New York

Wiedemann H (2015) Particle Accelerator Physics, Fourth Edition, Springer International Publishing Switzerland, Switzerland

7. CURRICULUM VITAE

Name Surname : Umut Keskin
Place and Date of Birth : TEKİRDAĞ 14.06.1991
Universities
- Bachelor's Degree : Abant Izzet Baysal University
e-mail : umutkeskin59@gmail.com
umut.keskin@cern.ch
Address : Bahçelievler Mahallesi Çiğdem Sokak Çağdaş Sitesi Daire 9 BOLU/Merkez

Projects :

- Scientific and Technological Research Council of Turkey (TUBITAK) TAU-shoWER (TAUWER) Project, Grant Number: 114F138, (2015-2017), Researcher
- Ankara Institute of Accelerator Technologies & CERN - CLIC Beam Dynamics and Beam-Beam Interaction Studies Project, Grant Number: 2013TAEKCERN-A5.H2.P1.01-24, (2013-2018), Researcher

Schools :

- Tenth International Linear Accelerator School for Linear Colliders, December 8-19, 2016, KEK and Teijin Academy Fuji, JAPAN

Presentations (Major) :

- CLIC Beam Physics Meeting, Design and Beam Dynamics Studies for the Primary 5 GeV e- Driver Linac, Geneva, Switzerland, 2 March 2017

- CLIC Workshop 2017, Oral Presentation, Design and Beam Dynamics Studies for the Primary 5 GeV e- Driver Linac, Geneva, Switzerland, 6 March, 2017

- CLIC Beam Physics Meeting, Update on the Electron Driver Linac for the CLIC Positron Source, Geneva, Switzerland, 2 November 2017

List of Publications :

- K. Y. OYULMAZ, **U. KESKİN**, Ş. ATİK YILMAZ, A. YILMAZ VE H. DENİZLİ "CORSIKA Benzetim Programı Kullanılarak Çok Yüksek Enerjili Yukarı Yönlü Tau Nötrino Sağanakların Tespiti ve Tetiklemenin Belirlenmesi" Hızlandırıcı ve Algıç Fiziği Çalıştayı, 2016.
- Ş. ATİK YILMAZ, H. DENİZLİ, K. Y. OYULMAZ, **U. KESKİN**, A. YILMAZ "CORSIKA Benzetim Programı Kullanılarak Çok Yüksek Enerjili Yukarı Yönlü Tau Nötrino Sağanaklarının Çalışılması" Hızlandırıcı ve Algıç Fiziği Çalıştayı, 2016.
- K. Y. OYULMAZ, **U. KESKİN** VE H. DENİZLİ "Yukarı Yönlü Çok Yüksek Enerji Tau Nötrinonun Oluşturacağı Sağanakların Farklı Bozunma Mesafeleri ve Enerjierinde Özellikle π π^0 Bozunma Kanalı Kullanılarak Tespiti" XI. Ulusal Nükleer Bilimler ve Teknolojileri Kongresi, 2016

Awards :

- Poster Presentation Award:
  K. Y. OYULMAZ, **U. KESKİN** VE H. DENİZLİ "Yukarı Yönlü Çok Yüksek Enerjili Tau Nötrinonun Oluşturacağı Sağanakların Farklı Bozunma Mesafeleri ve Enerjierinde Özellikle π π^0 Bozunma Kanalı Kullanılarak Tespiti" XI. Ulusal Nükleer Bilimler ve Teknolojileri Kongresi ,2016 (**3rd Place**)